*Article*

Progress in Physical Geography
2016, Vol. 40(2) 247–275

DOI: 10.1177/0309133315615805
ppg.sagepub.com
SAGE

# Structure from motion photogrammetry in physical geography

**M.W. Smith**
University of Leeds, UK

**J.L. Carrivick**
University of Leeds, UK

**D.J. Quincey**
University of Leeds, UK

**Abstract**

Accurate, precise and rapid acquisition of topographic data is fundamental to many sub-disciplines of physical geography. Technological developments over the past few decades have made fully distributed data sets of centimetric resolution and accuracy commonplace, yet the emergence of Structure from Motion (SfM) with Multi-View Stereo (MVS) in recent years has revolutionised three-dimensional topographic surveys in physical geography by democratising data collection and processing. SfM-MVS originates from the fields of computer vision and photogrammetry, requires minimal expensive equipment or specialist expertise and, under certain conditions, can produce point clouds of comparable quality to existing survey methods (e.g. Terrestrial Laser Scanning). Consequently, applications of SfM-MVS in physical geography have multiplied rapidly. There are many practical options available to physical geographers when planning a SfM-MVS survey (e.g. platforms, cameras, software), yet, many SfM-MVS end-users are uncertain as to the errors associated with each choice and, perhaps most fundamentally, the processes actually taking place as part of the SfM-MVS workflow. This paper details the typical workflow applied by SfM-MVS software packages, reviews practical details of implementing SfM-MVS, combines existing validation studies to assess practically achievable data quality and reviews the range of applications of SfM-MVS in physical geography. The flexibility of the SfM-MVS approach complicates attempts to validate SfM-MVS robustly as each individual validation study will use a different approach (e.g. platform, camera, georeferencing method, etc.). We highlight the need for greater transparency in SfM-MVS processing and enhanced ability to adjust parameters that determine survey quality. Looking forwards, future prospects of SfM-MVS in physical geography are identified through discussion of more recent developments in the fields of image analysis and computer vision.

**Keywords**

Structure from motion, Multi-View Stereo, topographic survey, point cloud

## I Introduction

Over the past few decades advances in surveying technology have revolutionised our ability to record and characterise the Earth's surface

**Corresponding author:**
M.W. Smith, School of Geography and water@leeds, University of Leeds, Woodhouse Lane, Leeds, West Yorkshire LS2 9JT, UK.
Email: m.w.smith@leeds.ac.uk

quantitatively: a fundamental requirement of physical geography. Differential Global Positioning Systems (dGPS) and Total Stations (TS) have enabled 3D positioning of observations to millimetre-scale accuracy. More recently, Airborne Laser Scanning (ALS) and Terrestrial Laser Scanning (TLS) have increased the spatial coverage and density of available datasets through non-selective sampling of millions or even billions of survey points to produce 3D point clouds. The impact on the study of physical geography and geomorphology in particular is well documented (Tarolli, 2014). Yet, a limitation to the more widespread uptake of ALS and TLS is the capital outlay and expertise required to acquire and operate these complex instruments.

In the past few years, Structure from Motion (SfM) has been demonstrated to have the potential to democratise 3D topographic survey by offering rapid 3D point cloud acquisition for minimal expense. Geomorphologists, and physical geographers more generally, have been quick to adopt SfM as seen by the recent and increasing proliferation of studies utilising and testing SfM (e.g. James and Robson, 2012; Westoby et al., 2012). SfM has been applied to a wide range of environmental problems, including monitoring glacier movement (Immerzeel et al., 2014; Ryan et al., 2015), quantifying soil loss and gully erosion (Eltner et al., 2014; Frankl et al., 2015), observing and tracking lava movement (Tuffen et al., 2013) and landslide displacement (Lucieer et al., 2013), monitoring coastal recession (James and Robson, 2012), surveying fluvial morphology (Javernick et al., 2014) including submerged surfaces (Woodget et al., 2014), characterising rock outcrops (Favalli et al., 2012) and quantifying aboveground forest biomass (Dandois and Ellis, 2013).

At this point, it is instructive to define what is meant by 'SfM'. Strictly speaking, Structure from Motion refers to only one element of the SfM workflow. Although there are cases where a SfM-derived point cloud is seen as the end-product (Dandois and Ellis, 2010; Fonstad et al., 2013), the majority of studies then implement Multi-View Stereo (MVS) photogrammetry algorithms to increase the point density by several orders of magnitude. As a result, the combined workflow is more correctly referred to as 'SfM-MVS'.

To date there is no comprehensive synthesis of the practical options available to physical geographers when planning a SfM survey, errors to be expected from each choice and, perhaps most fundamentally, the underlying processes actually taking place as part of the SfM workflow. In this paper we provide a qualitative comparison of SfM-MVS with other field topographic survey techniques. We detail the origin of SfM-MVS and the workflow applied by many SfM-MVS software packages (Section III) and review the practical details of implementing SfM-MVS by outlining a number of choices (e.g. camera, survey platform, SfM software) to be made by the user (Section IV). Here we provide specific guidance on data acquisition for SfM-MVS users in physical geography. Existing validation approaches are synthesised (Section V) to provide an overview of the achievable quality of the resulting point clouds. We summarise a range of applications of SfM-MVS in physical geography (Section VI) and consider briefly potential future directions and opportunities for SfM-MVS to make important contributions to the discipline (Section VII).

## II The place of SfM in topographic survey

In recent decades there has been a gradual increase in our ability to collect topographic survey data, from $10^1$–$10^2$ measurements per day with a traditional optical level, increasing to $10^3$–$10^4$ with dGPS and to $>>10^6$ measurements per day with laser scanning technology. Improvements in precision and accuracy have been notable, but more modest. Each new

development has required new technology that is typically very costly (often >£10,000); conversely, SfM-MVS can offer similar data quality to high resolution survey techniques at minimal expense. A broad comparison of SfM-MVS with existing survey techniques is summarised in Figure 1.

TS or Electronic Distance Measurement (EDM) surveys offer high-accuracy point data (~mm 3D accuracy) of the ground surface (Fuller et al., 2003; Milne and Sear, 1997). Where local benchmarks or ground control is available, real-world co-ordinates can be provided, even in conditions where sky-view is limited as no communication with satellites is required. They are typically used in conjunction with a pole-mounted prism or can be used without a reflector. TS points are sampled selectively by the operator(s) and can be strategically positioned to identify notable breaks of slope, providing a high quality digital elevation model (DEM) for relatively small file sizes. The main disadvantage of TS surveys is the point density achievable within a survey campaign, which is limited by the time required to sample points individually. Moreover, the expert judgment of where to locate each survey point may introduce bias towards accessible locations and variability between operators (Bangen et al., 2014a). Such bias is significant because the interpolation that is required to produce a topographic model is affected by the specific survey point geometry.

Data provided by dGPS surveys can be of similar accuracy to that of TS surveys (Bangen et al., 2014b), depending on the length of time a point is occupied and survey mode. Real-time kinetic (RTK) surveys are commonplace in physical geography where a direct radio or GSM (mobile network) link between a surveyor and a base station can provide the surveyor with information on the final accuracy of the solution relative to the base station co-ordinates (Brasington et al., 2000, 2003; Wheaton et al., 2010). As such, dGPS surveys are subject to

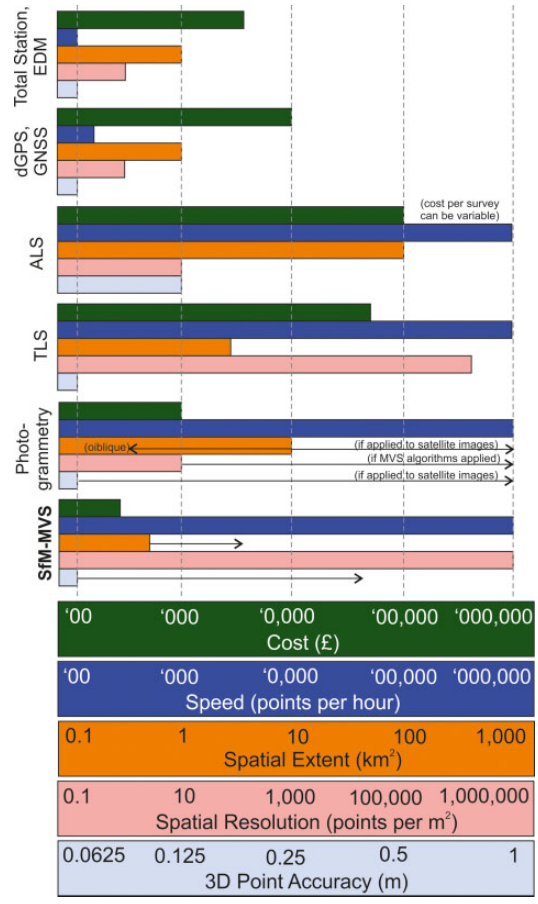


**Figure 1.** Comparison of digital survey methods with regard to financial cost, data acquisition rate, spatial coverage, resolution and accuracy. Note that photogrammetry and SfM values are dependent on survey range. Colour bars for photogrammetry represent 'conventional' aerial photogrammetry, though the range values for alternative implementations of photogrammetry are indicated. Bars derived from information in Brasington et al. (2000), Young (2012), Gallay (2013) and Bangen et al. (2014b).

many of the same advantages (accuracy, precision, selectivity) and disadvantages (low point density) as TS surveys (Bangen et al., 2014b). The accuracy of RTK-dGPS surveys is ~cm scale (higher accuracies can be achieved on continuously logging static mode) and is dependent on the number and geometry of satellites used

to compute a point, therefore a clear sky-view is also required. However, unlike TS surveys, a direct line-of-sight between the instrument and the survey pole is not required.

ALS, also known as airborne Light Detection And Ranging (LiDAR), has become a well-established survey tool in physical geography over the last two decades (e.g. Charlton et al., 2003; Evans and Lindsay, 2010; Thommeret et al., 2010). The remote platform and consequent large survey range (typically 100–4000 m between the sensor and object of interest; Gallay, 2013) means that ALS is naturally suited to landscape scale surveys, resulting in decimetre scale point resolution and accuracy (Bangen et al., 2014b; Gallay, 2013). TLS comprise essentially the same technology mounted statically on a conventional survey tripod (Brasington et al., 2012; Hetherington et al., 2005; Smith, 2015) (though mobile systems are also in use; Alho et al., 2009). The shorter range and static setup of TLS means that mm-scale precision and accuracy can be achieved. The main advantage of LiDAR systems is the acquisition rate, which can be up to hundreds of thousands of points per second. While TLS offers much higher survey accuracy and point density than ALS, this comes at the expense of reduced survey area. Moreover, both ALS and TLS are expensive survey solutions (>£30,000 for a TLS) that produce large quantities of data which must then be decimated to produce useful terrain products. Another disadvantage of TLS is portability; while the TLS instruments themselves typically weigh 5–10 kg, they require much ancillary equipment (e.g. tripods, batteries, cases, targets) and the total weight of many systems restricts their application to areas with good access. Where targets are used to register multiple scans together, surveys must be planned carefully such that they can be viewed from multiple scan locations. Time-limitations determine the number of tripod setups possible meaning that gaps or shadows may be present in the final point cloud owing to occlusion effects. Hand-held mobile laser scanners have been recently used to overcome the limited portability of tripod-mounted TLS (James and Quinton, 2014), though reported errors are centimetre-scale.

Conventional photogrammetry is the closest existing technique to SfM-MVS, and has contributed much to the workflow of SfM-MVS (Micheletti et al., 2015). Conventional photogrammetry uses precise knowledge of the 3D location and pose of cameras, or the 3D location of a set of control points located in the scene of interest, to reconstruct scene geometry. Achievable spatial resolution is a function of the pixel size but digital photogrammetry has been applied across a range of scales from plots of $\sim 10^1$ m$^2$ (Butler et al. 2002; Carbonneau et al., 2003) to landscapes or river reaches of $>10^6$ m$^2$ (Lane, 2000; Westaway et al., 2000). For photogrammetry, once equipment has been set up, data collection requires only several minutes. While vertical (overhead) photographs are required in conventional approaches, oblique images can be used either through the implementation of rotation matrices (Chandler, 1999) or by using more recent photogrammetric software capable of processing oblique images (James et al., 2006). Fine resolution and accurate (mm-scale) topography can be obtained at ranges of several metres; the achievable accuracy is reduced with increasing distance between the camera and object of interest. However, the main disadvantages of conventional photogrammetry are the degree of expertise required, the difficulty and expense of obtaining the large amount of a priori information required and the relative inflexibility of the image geometry (e.g. degree of overlap) which may render it unsuitable for some applications.

SfM-MVS is a non-selective survey method (like ALS, TLS and conventional photogrammetry where each data point is not selected for inclusion in the survey individually by the surveyor) and the resulting data are most similar to those of TLS. Similar (or greater) point densities can be achieved and while point precision

and accuracy is mostly determined by survey range, sub-cm scale errors are achievable (Smith and Vericat, 2015). Perhaps the biggest disadvantage of SfM-MVS is the fact that the quality of the resulting surface model depends on many different factors related to an individual survey. SfM-MVS data are typically not as precise as TLS-derived point clouds; however, SfM-MVS is flexible enough to be applied at a wide range of scales. Specifically, to date, it has been used over survey areas from $10^{-2}$–$10^{6}$ $m^2$ (Smith and Vericat, 2015) and was even used by Dietrich (2015) to survey downstream morphological patterns in a 32 km river reach. The equipment needed for SfM-MVS is often portable and while scale can be provided using only non-specialist technology (e.g. standard laser rangefinders), accurate scaling and georeferencing requires the use of a TS or dGPS. Occlusion and shadowing remain an issue with SfM-MVS, but it is minimised relative to TLS surveys owing to the greater number of viewpoints that can be integrated into a single SfM-MVS survey.

It is clear that each of the techniques outlined above has different strengths and weaknesses and is better suited to different tasks. Certainly, SfM-MVS is not a complete substitute for these other methods (for example, accurate fluvial bathymetry over small areas is better obtained by TS or dGPS survey than SfM-MVS; Bangen et al., 2014b; Woodget et al., 2014). However, in some circumstances, particularly where plot scale ($\sim 10^{1}$ $m^2$) data is required (Smith and Vericat, 2015) or where decimetre scale accuracy is acceptable over $\sim 1$ $km^2$ of bare ground (Javernick et al., 2014), SfM-MVS is an efficient and cost-effective survey method.

## III Principles underlying SfM-MVS

The clear similarities between conventional photogrammetry and SfM-MVS may lead to the assumption that SfM-MVS is simply an incremental development in photogrammetry. However, several aspects of SfM-MVS have a different origin entirely, stemming instead from advances in 3D computer vision algorithms. Nonetheless, photogrammetric principles and techniques are embedded in the SfM-MVS workflow (see Micheletti et al., 2015). The typical workflow implemented by many SfM-MVS software packages is presented and summarised in Figure 2. The specifics of this workflow will vary from one software package to another, but there exists a clear commonality. The description here is predominantly qualitative to best communicate a technical workflow to a broad audience. Interested readers are directed to other sources (Hartley and Zisserman, 2003; Lowe, 2004; Snavely, 2008; Szeliski, 2011; Triggs et al., 2000) for specific details of the mathematical operations applied.

### *1 Feature detection*

With a set of images of a scene taken from multiple viewpoints, the first step is to identify features (or 'keypoints') in each image and assign a unique identifier to these regardless of the image perspective or scale. To be most useful for SfM-MVS this keypoint identification should be valid for images taken at relatively wide baselines (i.e. different perspectives). Identification of sets of pixels that are invariant to changes in scale and orientation and suitable for wide-baseline matching has been a longstanding question in computer vision (Szeliski, 2011). Popular feature detection algorithms improve on traditional correlation-based approaches as they geometrically normalize the region containing the feature and correct for photometric distortions (e.g. illumination) to ensure rotational and photometric invariance (Mikolajczyk et al., 2005). While there are several alternative methods for identifying features (including SURF (Bay et al., 2008), ASIFT (Morel and Yu, 2009), BRIEF (Calonder et al., 2010) and LDAHash (Strecha et al., 2012)), the Scale Invariant Feature Transform (SIFT) object recognition system is used most widely in SfM (Lowe, 1999, 2001, 2004) and has

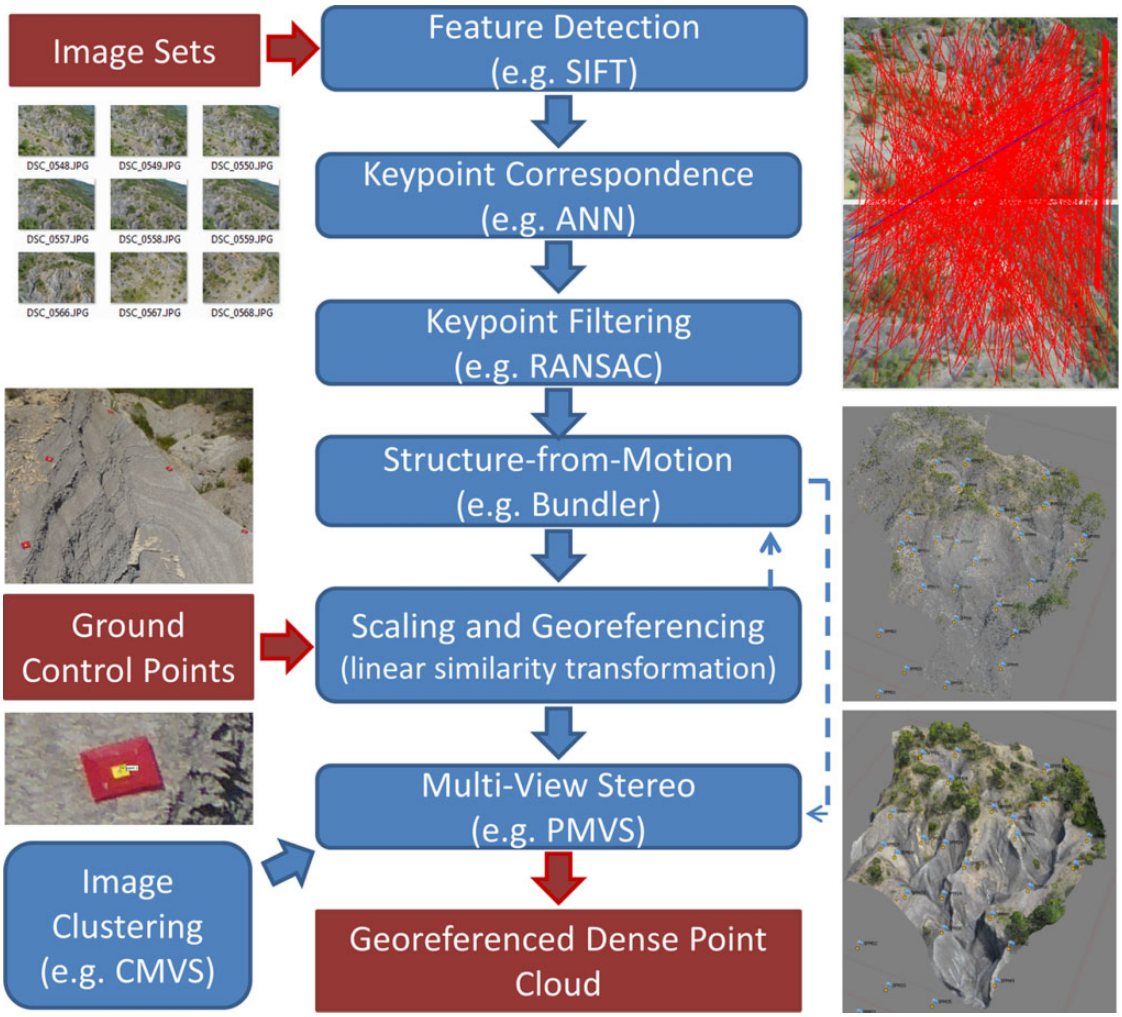


**Figure 2.** Typical workflow in the production of georeferenced dense point clouds from image sets and ground control points. Inputs and outputs are shown in dark red. In the top right, as a demonstration, matches determined to be valid are shown in red, while matches determined to be invalid are given in blue.

been shown by Lowe (2004) to perform well for changes in viewpoint of <40°.

## 2 Keypoint correspondence

The next step requires the identification of correspondences between keypoints in multiple images. Of course, there is no guarantee that each keypoint will be represented in each image, so a threshold to identify matches is applied. Descriptors are typically complex (for example, the SIFT descriptor uses 128 vectors to describe each point). The ratio of the Euclidean distance of the nearest neighbour with that of the second nearest is termed the 'distance ratio' and a minimum value (typically 0.6–0.8; Snavely et al., 2008) is specified to increase the chance of all matches being correctly identified. In such high-dimensional space, a brute-force Euclidean nearest neighbour search is computationally

demanding (Arya et al., 1998). *k*-dimensional trees (or *k-d* trees) modified for approximate matching (Muja and Lowe, 2009) are applied as an efficient and approximate solution to this problem. These binary trees partition multidimensional data to quickly eliminate large search spaces (Bentley, 1975; Friedman et al., 1977). The Approximate Nearest Neighbour (ANN) solution permits relative error in the identification of the nearest neighbour (Arya et al., 1998) and by searching only the top ranked candidates can make substantial time savings.

## 3 Identifying geometrically consistent matches

A further filter of keypoint correspondences is then applied to try and identify and remove any remaining erroneous matches. Taking any image pair with multiple common keypoints, the fundamental matrix (F-matrix) can be calculated using the Eight-point algorithm (Longuet-Higgins, 1981). The F-matrix specifies the relationship between the two images and reconstructs the scene up to a projective transformation where all points lying on a single line will remain aligned in this way (i.e. 'collinearity' is preserved). Candidate F-matrices are evaluated using the RANdom SAmple Consensus (RANSAC) method (Fischler and Bolles, 1981) in which keypoints used in the construction of the F-matrix are randomly sampled and the difference between the returned F-matrix and that returned by other sampled keypoints is computed. Beyond a threshold the keypoint is considered an 'outlier' and not part of the model fit. Sampling is repeated on different subsets until there is a 95% chance that the subset contains only 'inliers' for which the F-matrix is returned. After further refinement, all 'outlier' matches are removed. Other similar 'hypothesise-and-test' frameworks may be implemented at this stage, such as the Maximum Likelihood Estimation Sample Consensus (Torr and Zisserman, 2000) or the Hough transform (Ballard and Brown, 1982).

## 4 Structure from motion

From the geometrically correct feature correspondences, SfM uses bundle adjustment algorithms to simultaneously estimate the 3D geometry (or structure) of a scene, the different camera poses (extrinsic calibration) and the camera intrinsic parameters (intrinsic calibration) (Ullman, 1979). Whereas conventional photogrammetric techniques share this step, they often require separate camera calibration. Where such camera calibration is unavailable, SfM uses both EXIF tags in the images and the redundancy provided by the large number of images and keypoint correspondences to estimate the intrinsic camera parameters that define the camera calibration matrix (e.g. skew, focal length, principal point and often radial distortion parameters). By minimizing a cost function, bundle adjustment results in *jointly optimal* 3D structure and camera parameters (see Granshaw (1980) and Triggs et al. (2000) for detailed reviews). Here, 'bundle' refers to the bundles of light rays connecting camera centres to 3D points, and 'adjustment' refers to the minimisation of a non-linear cost function that reflects the measurement error (Szeliski, 2011). This error term can incorporate many sources of information including errors in the projection of individual image features in the object space (re-projection errors).

Parameter values must be assigned initial values before a non-linear parameter optimisation of the bundle adjustment is calculated. Sequential methods take an initial pair of images, which typically exhibit many common keypoints and a wide baseline, and initialize the camera intrinsic parameters from EXIF tags and use the Five-point algorithm (Nistér, 2004) to estimate the F-matrix. Incorrectly specified initial parameters for an image can yield an optimisation to local minima instead of the 'correct' solution and cause that image to be rejected from the project. Tracks between keypoints are then triangulated to give initial estimates of

feature positions (see Hartley and Sturm, 1997). Errors between the projections of each track and the corresponding keypoints are minimized as part of a two-frame bundle adjustment. The camera containing the largest number of tracks whose 3D locations are already known is then selected and added into the optimization. Using these known 3D locations the 2D co-ordinates of the new image are mapped into the 3D object space and the intrinsic camera parameters estimated. In many SfM implementations, a further bundle adjustment is run with only the new parameters permitted to change. At each stage, keypoints with a high re-projection error are removed. With each image added sequentially, a global bundle adjustment is then performed to refine the entire model.

## 5 Scale and georeferencing

The output of the SfM stage is a sparse, unscaled 3D point cloud in arbitrary units along with camera models and poses. A minimum of three ground control points (GCPs) with XYZ co-ordinates are required to scale and georeference the SfM-derived point cloud using a seven parameter linear similarity transformation; i.e. three global translation parameters, three rotation parameters and one scaling parameter (Dandois and Ellis, 2010; James and Robson, 2012). Unlike conventional photogrammetry, each photograph does not need to contain visible GCPs; dGPS or TS surveys can provide the co-ordinates of targets clearly visible in the imagery. A much larger number of targets than three is recommended; the minimum absolute number depends on the size of the survey area, but they should cover the whole extent of this area (Javernick et al., 2014; Smith et al., 2014) and be well distributed throughout the area (James and Robson, 2012). Alternatively, 'direct' georeferencing and scaling can be performed from known camera positions derived from RTK-GPS measurements and an Inertial Measurement Unit (Tsai et al., 2010; Turner et al., 2014). A common hybrid of the two georeferencing approaches uses direct georeferencing to provide approximate camera locations to initialize the bundle adjustment and then uses external GCPs to better constrain the solution (e.g. Rippin et al., 2015; Ryan et al., 2015).

## 6 Refinement of parameter values

The identification of GCPs and input of their co-ordinates in the preceding step provides additional information of the 3D geometry that can be used to further refine intrinsic camera parameter estimates and reconstructed scene geometry. The known co-ordinates (and estimates of point error) provide an additional source of error in the minimization of the non-linear cost function during the bundle adjustment step. With this external information included in the model, the bundle adjustment can be re-run to optimize the image alignment in light of this new information by minimizing the sum of the re-projection error and the georeferencing error. The spatial distribution of GCPs throughout the survey area is critical for this process to be effective.

## 7 Multi-view stereo image matching algorithms

The final step in the workflow is the application of MVS algorithms to the already scaled and georeferenced sparse point cloud and camera parameters. MVS usually increases the density of the point cloud by at least two orders of magnitude. As detailed by Seitz et al. (2006), there are a wide variety of MVS algorithms, which can be classified into: (i) Voxel-based methods which are 3D grids that are occupied to define the scene, e.g. Seitz and Dyer (1999); (ii) surface evolution-based methods that use iteratively evolved polygonal meshes, e.g. Furukawa and Ponce (2009); (iii) depth-map merging methods where individual depth maps (showing the distance between the camera

viewpoint to the 3D scene objects) are combined into a single model, e.g. Li et al. (2010a); and (iv) Patch-based methods where collections of small patches or surfels represent the scene, e.g. Lhuillier and Quan (2005). A commonly applied method in physical geography applications is the patch-based MVS (PMVS) algorithm of Furukawa and Ponce (2010); in comparisons against other MVS algorithms (Ahmadabadian et al., 2013), this MVS method performs well. In general, PMVS matching of features requires reliable texture information, the lack of which may result in gaps in the final model. Once matched, patches are then grown around identified matches. By accounting for occlusion in the model, visibility constraints are then used to filter out outlier patches.

As the final step of MVS is computationally burdensome when a global reconstruction is specified (Pons et al., 2007), there is the option to split a project into overlapping clusters of images to reduce random-access memory (RAM) requirements. Each cluster is then run through the dense MVS reconstruction separately. Furukawa et al. (2010) detail such an image clustering method, known as Clustering Views for Multi-View Stereo (CMVS). As demonstrated for a physical geography application of SfM-MVS by Dietrich (2015), the addition of an image clustering step improves the scalability of MVS, permitting much larger numbers of images to be processed within any given run time.

Throughout Steps 1–7 above, thresholds and parameters are used to distinguish correct matches from incorrect matches and prevent the excessive computational burden that would be required for exhaustive nearest neighbour searches in the matching of keypoints in each image. The specific values will be variable between different SfM-MVS packages. A typical SfM-user may not be able to adjust these values, may be unaware of this or may simply adjust a qualitative global accuracy setting implemented within particular SfM software packages, or use default values. Moving beyond such a 'black box' approach, an understanding of the full SfM-MVS workflow implemented is useful for physical geographers to identify and minimize potential sources of error in the resulting topographic data.

## IV SfM in practice

The flexibility of the SfM-approach is advantageous considering the range of problems in physical geography to which it can be applied. However, one consequence of this flexibility is that practitioners are faced with many choices in the design and implementation of a SfM-MVS survey.

### *1 Platforms*

Most imagery can be used for SfM-MVS; indeed the SfM package outlined in Snavely et al. (2008) was designed to use collections of independent images extracted from image searches on the internet. A range of options are available, from ground-based imagery to fully airborne solutions (Figure 3). In general, there are trade-offs between: (i) pixel resolution; (ii) spatial coverage; (iii) image quality; and (iv) cost-effectiveness.

Hand-held ground-based solutions are the most inexpensive option (only a camera and georeferencing method is needed), can provide excellent pixel resolution and image quality and are easy to implement. The key disadvantage of hand-held solutions is that they are typically limited to the plot-scale ($\sim 10^1$ m$^2$). However, with high relief (e.g. an incised valley or cliffs) areas approaching one hectare can be surveyed from the ground (James and Quinton, 2014; Micheletti et al., 2014; Smith et al., 2014). Matching of oblique ground-based images over large areas can be unreliable on relatively flat terrain; isolated mismatched areas are apparent in the final point clouds, which must be inspected carefully (Smith and Vericat, 2015). Extendable masts, booms (Figure 3d) or mobile inspection poles can be used to raise a camera up to 20 m above ground to reduce the likelihood of such

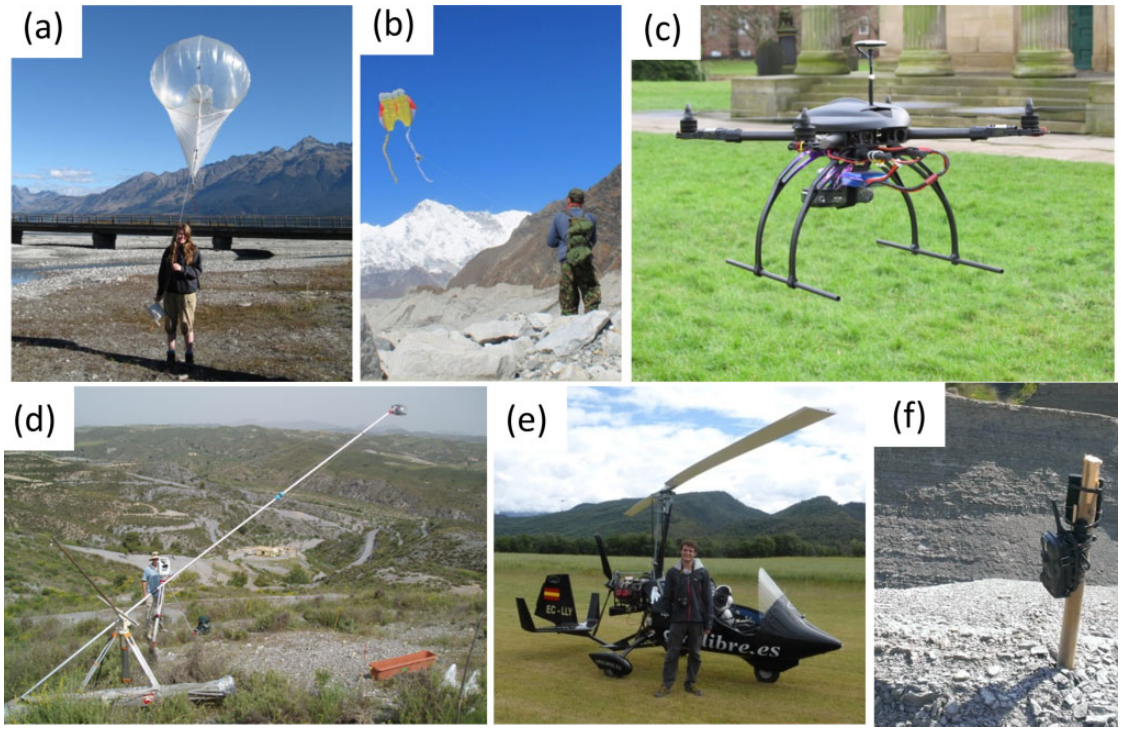


**Figure 3.** Examples of platform-types from which SfM-MVS imagery can be applied: (a) lighter-than-air blimp; (b) kite; (c) multicopter-type UAV; (d) camera boom; (e) gyrocopter; (f) trail camera.

mismatches by gaining a more advantageous viewpoint. However, on-the-ground image swaths are still limited in spatial extent and retaining stability of a pole or mast in adverse weather can be challenging.

Lighter-than-air blimps (Figure 3a) can raise a camera higher still, up to 500 m, though they can become difficult to position if the wind speed exceeds $\sim$15 km $h^{-1}$ (Verhoeven et al., 2009). Mobile blimp systems are a low-cost solution (Vericat et al., 2009) but are limited in their payload capability, constrained to operating loads of between 0.25–0.5 kg per 1 $m^3$ of lighter-than-air gas. They also cannot be deployed in high winds and may require a local source of suitable gas. Conversely, kites (Figure 3b) can carry a payload of several kilograms. Irregular or light winds can make controlling kite-based systems challenging; thus, some systems integrate blimp and kite components to improve the range of suitable weather conditions.

There has been a proliferation in low-cost airborne platforms in recent years; unmanned aerial vehicles (UAVs) have been used extensively for acquisition of SfM-MVS imagery (e.g. Lucieer et al., 2014; Tonkin et al., 2014; Woodget et al., 2014). There exists a wide range of UAVs (see Colomina and Molina, 2014) from self-propelled fixed-wing aircraft to airships. The most popular UAVs have been so-called 'multicopters' (including quadcopters, hexacopters or octocopters; Figure 3c) because of their ease of operation, stability in most weather conditions and recent decline in financial cost. Most multicopters can take a payload of several kilograms, though larger systems may take up to 10 kg (Lejot et al., 2007). Flight control software and units can allow pre-programmed routes to be

followed (Oúedraogo et al., 2014). On smaller UAVs, image quality can be compromised by blurring from vibrations (Dunford et al., 2009), although use of a gimballed-camera mount can minimise this problem. In many countries legislation limits the range and ground-type over which UAVs can be flown. In general, UAVs have a lower maximum altitude than blimps or kites. In each case, the flying altitude chosen will determine the final pixel resolution for a specific camera.

The broadest spatial coverage can be achieved with a commissioned, piloted overflight in an aircraft, often a helicopter (Dietrich, 2015; Javernick et al., 2014). This removes maximum altitude restrictions (though minimum altitude restrictions apply) and permits a greater flexibility and responsiveness in the survey to ensure full coverage. As with UAVs, higher altitude surveys will improve spatial coverage at the expense of pixel resolution. Issues with vibrations and blurring are circumvented when images are taken manually, though this is not always possible. Cost is a disadvantage of the piloted helicopter approach. Much smaller light aircraft (James and Varley, 2012), microlites (James and Robson (2012) with images from Cecchi et al. (2003)) or piloted gyrocopters (Smith and Vericat, 2015; Figure 3e) offer a more cost-effective solution and can be hired for <£200 per hour.

## 2 Sensors

Images for SfM-MVS can be acquired from almost any camera system; and consequently there is a spectrum of image quality. At the lower quality end are still frames extracted from video. Lower pixel counts, blurring, camera lens and image stability issues mean that still frames captured from video produce poor quality 3D data (Thoeni et al., 2014). Where sensors employ a rolling shutter (e.g. GoPro cameras), not all parts of the resulting images are recorded at the same instant, which is a problem for SfM-MVS analysis when the sensor is mounted on a moving platform.

However, comparisons between simple low-cost cameras (such as those embedded in smartphones or compact cameras) and expensive digital SLRs do not show significant differences in point cloud quality at short ranges (Micheletti et al., 2014; Thoeni et al., 2014). Intrinsic camera parameters are most easily defined for wide-angle lenses (equating to around 35 mm on a traditional SLR) whereas those with longer lenses (>55 mm) or fish-eye lenses require bespoke calibration models (Micusik and Pajdla, 2006). Image resolution and sharpness becomes more important at longer survey ranges, i.e. >100 m. Cameras with larger imaging sensors are advantageous for high-altitude aerial imagery, providing a better dynamic range, finer detail and less noise (Cramer, 2004). Moreover, larger sensors (e.g. Full Frame 35 mm format) capture larger image areas at a given focal length, increasing on-the-ground image swaths. The camera platform must be considered, as camera size and weight will be of importance for some aerial platforms. Where the operator is not physically present to capture the images manually, a triggering mechanism is required that can be achieved with remote shutter releases (wired / wireless) or intervalometers (internal / external) (e.g. Vericat et al., 2009). For longer-term deployment, arrays of inexpensive trail cameras can be installed to obtain regular synchronised images of a scene (James and Robson, 2014b) (Figure 3f).

## 3 Data acquisition

When acquiring images for SfM-MVS, the main goal is to capture the scene of interest from as many different viewpoints as possible. Advice on SfM-MVS image acquisition for specific applications is given in several papers, including Favalli et al. (2012); James and Robson (2012); Westoby et al. (2012); Bemis et al. (2014); Micheletti et al. (2014); Smith et al., (2014) and Stumpf et al. (2015). In summary,

the following practical guidance should assist the planning of SfM-MVS data acquisition:

- Full 360° coverage is ideal (Westoby et al., 2012), though not always necessary so long as all surfaces of interest are visible in multiple photographs.
- While SfM can sometimes work with two input images (James and Robson, 2014b), a much larger number of images is recommended. While the exact number will depend on the scene size and complexity, tens to hundreds of pictures are often used (Favalli et al., 2012).
- Higher quality input images can result in higher quality model output (Bemis et al., 2014); however, large images may need to be re-sized to reduce processing times (Westoby et al., 2012).
- Overlap between images is best considered in terms of both coverage and angular change as multiple images taken of a surface from the same camera location do not aid the reconstruction (Favalli et al., 2012).
- Angular changes of >25–30° between adjacent camera locations should be avoided because identification of correct keypoint correspondence is limited for larger changes of perspective (Moreels and Perona, 2007). Maximum angular changes of 10–20° are advisable (Bemis et al., 2014).
- Each point on the surface must be visible in at least two images, but again, more is clearly preferable to ensure that all locations are reconstructed successfully.
- Large jumps in image scale are best avoided (i.e. avoid mixing close up imagery with that taken from a large range without also including intermediate scale imagery) as image textures will appear differently at different scales and prevent accurate matching (Bemis et al., 2014).
- Avoid using zoom lenses and changing focal lengths; while not essential, keeping camera parameters constant can aid the bundle adjustment in some SfM-MVS packages.
- The interval between images should be minimised as changes to lighting conditions and shadow locations will interfere with keypoint matching (James and Robson, 2012).
- Mobile elements in a scene should be avoided as keypoint matching algorithms rely on a static scene. Where flexible vegetation or other dynamic elements are present, this may be challenging, especially in shifting winds (Bemis et al., 2014). Components of the mobile camera platform (e.g. helicopter skids, kite tethers) or the camera operator (i.e. feet) should be avoided for the same reason.
- Scenes devoid of distinct features (e.g. smooth ice surfaces) will be challenging and often produce fewer keypoint correspondences and lower point densities (Westoby et al., 2012).
- Shiny or reflective surfaces are similarly unsuitable for SfM-MVS as their apparent features change with camera position.
- Where exclusively vertical imagery is collected, a doming effect can be observed (Oúedraogo et al., 2014; Rosnell and Honkavaara, 2012) as a result of incorrect specification or determination of the camera intrinsic parameters. Taking slightly off-vertical convergent imagery and designing a distributed network of GCPs can partially correct this doming (James and Robson, 2014a; Smith and Vericat, 2015).
- The maximum number of images for SfM-MVS analysis will be determined by logistical and computational capabilities. With increasing image numbers, gains from adding further imagery are reduced substantially as the percentage

of surface points that are already visible in three or more images increases, though this depends on the geometric arrangement of the image set as a whole.

For scaling and georeferencing, clearly visible targets (GCPs) are required that can be identified in the images. The bigger the target, the better it will be seen from a distance, but also the greater the error in defining the exact reference point, which may be located at the centre of such a target. Targets should be placed on stable features, be visible in as many images as possible (certainly a minimum of three images) and be easily distinguishable from the surrounding landscape. There is no requirement for GCPs to be visible in every image used. Distribution of GCPs through the area of interest determines the quality of the final model (James and Robson, 2012) and can help to mitigate doming (James and Robson, 2014a); these should ideally cover both the margins and the centre of the scene, covering a good range of values in each spatial dimension. Linear configurations of GCPs should also be avoided. High quality 3D co-ordinates of these GCP points (from dGPS or TS surveys) are preferable. Alternatively, co-ordinates of camera positions derived from RTK-GPS measurements and an Inertial Measurement Unit can be used to directly georeference SfM-MVS point clouds (Turner et al., 2014).

## 4 Software

A number of SfM-MVS packages exist, ranging from web-based services to open-source and commercial software.

Freely available web-based services include Autodesk 123DCatch/ReCap (http://www.123dapp.com/catch), Microsoft Photosynth (https://photosynth.net/) and ARC3D (http://www.arc3d.be). Both Photosynth and 123DCatch are available as either mobile application or desktop versions. In all cases, post-processing options are limited and require export to other software for processing, cleaning or editing (e.g. Meshlab, http://meshlab.sourceforge.net/). In the case of Photosynth, the generation of dense point clouds requires additional software (e.g. PMVS2, see below). ARC3D is typically used for cultural heritage projects, while both Photosynth (Fonstad et al., 2013; James and Varley, 2012) and 123DCatch (Gómez-Gutiérrez et al., 2014; Micheletti et al., 2014) have been used for physical geography applications.

Open-source code packages are used regularly for SfM. The combination of Bundler (http://www.cs.cornell.edu/~snavely/bundler/) (Snavely, 2008; Snavely et al., 2008) for sparse cloud generation and Patch-based Multi-View Stereo (PMVS2) (http://www.di.ens.fr/pmvs/) (Furukawa and Ponce, 2010) for dense cloud production is a common workflow (James and Robson, 2012). As Bundler does not exploit modern graphics processing units (GPUs) it can be slower than commercially available alternatives. Moreover, designed for web-based photo tourism, it assumes that each image was taken from a different camera and uses a pin-hole camera model, which can produce lower accuracy results than with other models (Snavely et al., 2008). VisualSfM (http://ccwu.me/vsfm/) combines a SfM algorithm and PMVS (with associated image clustering software CMVS) into a single interface and is computationally faster. MicMac (www.micmac.ign.fr/) also comprises a full SfM-MVS workflow, offering complex models of camera intrinsic parameters. MicMac can include GCP information in the bundle adjustment step and has yielded accurate results (Oúedraogo et al., 2014; Stumpf et al., 2015). Ecosynth (http://ecosynth.org/) is another freely available SfM software used for vegetation mapping (Zahawi et al., 2015).

The most frequently applied commercially available software package is Agisoft Photoscan (http://www.agisoft.com/), which offers a user-friendly solution to SfM-MVS. Educational licenses can be purchased for ~£360.

Although post-processing options are currently limited, this has seen widespread application in physical geography (e.g. Javernick et al., 2014; Leon et al., 2015; Smith et al., 2014). Pix4DMapper (http://pix4d.com/) is an emerging software used in several soil erosion applications (Castillo et al., 2012; Eltner et al., 2014) and has been shown to perform well on bundle adjustment, but less well on dense matching and orthophoto generation (Unger et al., 2014). Educational licenses can be purchased for ~£1250. Eos PhotoModeler Scanner (http://www.photomodeler.co.uk/) (~£1600) has also been used in physical geography (Irvine-Fynn et al., 2014; Micheletti et al., 2014). Other available commercial software, including Autodesk ImageModeler (supplied free with other Autodesk software purchases; www.autodesk.com/imagemodeler) and D-Sculptor (£500) (http://www.d-vw.com/) require some manual feature matching and photogrammetric expertise.

While many open-source point cloud viewers are available, Meshlab (above) and CloudCompare (http://www.danielgm.net/cc/) are used commonly and provide substantial editing and post-processing functionality. Alternatively, SfM-MVS data can be imported into TLS-focused software (e.g. Leica Cyclone; RiSCAN PRO).

## 5 Filtering and digital elevation model (DEM) generation

Distinguishing between ground surface and non-surface points and normalizing the point density is often required for point clouds (Brasington et al., 2012). Extensive software libraries of point filters are available (e.g. the Point Cloud Library, www.pointclouds.org); however, the way in which particularly ground-based SfM-MVS data is captured limits the applicability of existing tools developed for ALS data as point densities are much higher and vegetation is captured from a different perspective. Radius-based methods of outlier detection are commonplace (Hodge et al., 2009). Geomorphologists and many other users typically wish to filter out vegetation from the point cloud and focus on the bare ground surface topography (Javernick et al., 2014); conversely, ecologists may wish to focus on the vegetation points alone, to estimate biomass, for example (Zahawi et al., 2015). Classification of vegetation and ground points is more challenging as they may be less easily distinguished. Brodu and Lague (2012) identify such points based on multi-scale dimensionality criteria. Use of colour filters is also possible, as SfM-MVS returns true-coloured points. Intelligent decimation algorithms (e.g. ToPCAT; Brasington et al., 2012; Rychkov et al., 2012) create gridded terrain products at a user-specified grid-scale, also returning sub-grid roughness statistics for each cell. Normalization of point density is a necessary step for the creation of raster-based topographic data products and reduces file sizes markedly as only summary statistics for each grid cell are required and details of individual points are discarded.

Finally, interpolation algorithms such as Inverse Distance Weighting, Radial Basis Functions or Ordinary Kriging (see Bell (2012) for a review) are required to fill any gaps in the SfM-MVS-derived model for DEM creation. Commercially available SfM-MVS software (e.g. Agisoft Photoscan) also offer DEM-creation tools. Development of efficient processing methods to extract the maximum useful data from 3D point clouds remains a research priority, as much essential information of the 3D scene (e.g. multiple elevation values at a single raster cell as seen with overhanging surfaces) is lost in the conversion into rasterised DEMs. In addition, orthophotos can be generated from point cloud data, often by running surfacing algorithms to generate a textured mesh, re-projecting the photographs onto the mesh and viewing the mesh from an orthographic projection. Such orthophotos yield additional information of use to physical geographers in many applications.

## V Validation of SfM-MVS

As with any emerging technology, quantitative validation of SfM-MVS-derived topographic data against those derived from more conventional methods (e.g. TS, dGPS, ALS, TLS) is prerequisite to confident application to a real-world problem. Only TLS and ALS provide directly comparable topographic data, but concurrent data derived using laser scanning is rarely available. Moreover, issues of beam divergence and 'mixed pixels' in laser scan data mean that in some cases there is no a priori reason to treat TLS data as the more correct data set, especially where SfM-MVS survey ranges (i.e. object-camera baselines) are short (Smith and Vericat, 2015).

Numerous studies have validated SfM-MVS-derived data against other methods; we have synthesised them herein to provide a broad overview of the capabilities of SfM-MVS. The dataset is compiled from the findings of Favalli et al. (2012), Harwin and Lucieer (2012), James and Robson (2012), Mancini et al. (2013), James and Quinton (2014), Javernick et al. (2014), Lucieer et al. (2014), Micheletti et al. (2014), Oúedraogo et al. (2014), Ružić et al. (2014), Smith et al. (2014), Thoeni et al. (2014), Tonkin et al. (2014), Smith and Vericat (2015), Stumpf et al. (2015), sub-aerial data from Woodget et al. (2014) and an unpublished result by the authors on ice surface plots. The aggregate dataset consisted of 50 data points covering a wide range of survey scales. Most studies reported the vertical Root Mean Squared Error (RMSE), Mean Error (ME) or Mean Absolute Error (MAE). ME values should be treated with caution, as positive and negative errors will compensate for each other.

Three general validation methods have been identified (see Smith and Vericat, 2015): (i) Point-to-Raster (PR), where a SfM-MVS-derived DEM is validated against point data from TS or dGPS (Javernick et al., 2014; Lucieer et al., 2013) and results depend on both the DEM grid-size and location of the validation point relative to the mean elevation within any cell; (ii) Raster-to-Raster (RR), where two separately derived DEMs are compared (Favalli et al., 2012; James and Robson, 2012) and the method of validation-DEM generation must be considered carefully to ensure comparability; and (iii) Point-to-Point (PP), where two point clouds are compared directly (James and Quinton, 2014) and a limiting assumption is that two points would be exactly concordant under error-free conditions. Analysis of the compiled dataset reveals that PP- and RR-type validation typically results in smaller errors than PR-type validation. Smith and Vericat (2015) showed that even at 0.1 m grid sizes, PR-type validation can yield RMSE vales $\sim$20% higher than RR-type validation of the same data. This discrepancy is to be expected since RR-type validation compares two rasters that both summarise the topographic variability within a single grid cell statistically, while PR-type validation compares the SfM-MVS-derived raster with a single point measurement taken within that grid cell which will exhibit sub-grid topographic variability. Other validation methods have been described: Favalli et al. (2012) use a mesh-comparison tool (Cignoni et al., 1998) instead of generating raster-based topographic models, while Lague et al. (2013) compute surface normals for each point based on all data points within a pre-specified radius to inform the comparison of points (as applied by Stumpf et al., 2015).

Over half of validation data points (56%) used ground-based imagery, while the remainder are based on imagery from airborne platforms (including manned and unmanned systems). The reported RMSE is an order of magnitude greater for aerial surveys (0.277 m) than ground-based surveys (0.043 m), but aerial surveys typically cover larger areas with the camera positioned at a greater distance from the object of interest (i.e. a longer survey range). Indeed, the main observable effect on SfM-

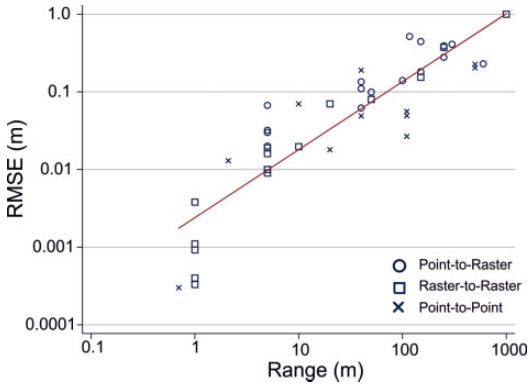


**Figure 4.** Variability of SfM-MVS Root Mean Squared Error (RMSE) with survey range (m) for different validation-types. Fitted power law described in the text. Data extracted from: Favalli et al. (2012); Harwin and Lucieer (2012); James and Quinton (2014); James and Robson (2012); Javernick et al. (2014); Lucieer et al. (2014); Mancini et al. (2013); Micheletti et al. (2014); Oúedraogo et al. (2014); Ružić et al. (2014); Smith et al. (2014); Stumpf et al. (2015); Thoeni et al. (2014); Tonkin et al. (2014); sub-aerial data from Woodget et al. (2014) and an unpublished result by the authors on ice surface plots. Adapted from Smith and Vericat (2015).

MVS data quality is a result of survey range (Figure 4). A linear degradation of precision with survey range might be expected from the increased pixel size; James and Robson (2012) observed such a linear relationship between the standard deviation of errors and survey range for three validation studies, estimating a ratio between these values as 1:1000. Yet RMSE is reported more commonly, it integrates all sources of error, and absolute accuracy is often required for monitoring studies. Considering RMSE and survey range, Micheletti et al. (2014) observed a ratio of 1:625. Combining the 43 validation data points that report RMSE, our data show a similar median ratio (1:639). A power law better describes the relationship between RMSE and range. The exponent of this relationship (0.88; $R^2 = 0.80$) is reasonably close to linear (Smith and Vericat, 2015).

Figure 4 provides a useful indication of errors expected for SfM-MVS surveys at a given range. However, the effect of validation method can be seen with PR methods exhibiting the highest errors for a given survey range. When survey range is taken into account, there are minimal differences between the accuracy of ground-based and aerial SfM-MVS surveys. Overall, considering the RMSE: range ratio, $\sim$10–15 mm errors are achievable at $\sim$10 m survey range suitable for detailed studies, while $\sim$100–200 mm errors are observed from 100 m range which could be applied over much larger areas. Such errors are similar to those expected from ALS surveys (Gallay, 2013).

Several studies included in the above analysis report results using multiple SfM-MVS workflows (e.g. varying cameras or software) on the same image set or area of interest (James and Robson, 2012; Javernick et al., 2014; Micheletti et al., 2014; Oúedraogo et al., 2014; Smith and Vericat 2015; Smith et al., 2014; Stumpf et al., 2015; Thoeni et al. 2014). In each case, the best-performing SfM-MVS-workflow on each image set or area of interest was selected for inclusion in Figure 4. Through comparison of the best-performing workflow with other workflows, these studies yield further insight into the effects of GCP distribution, processing software used and camera used for image acquisition.

Clearly, the GCP quality will determine overall SfM-MVS survey accuracy. In addition, it is well established that poor GCP distribution has a detrimental effect on survey quality. Javernick et al. (2014) reported an increase in RMSE from 0.23 m to 0.27 m when the study reach was extended beyond the area covered with GCPs. Smith et al. (2014) observed a more pronounced increase (from 0.14 m to 0.47 m). James and Robson (2012) also reported increased survey errors when GCPs were not distributed throughout the survey area.

In a comparison of SfM-MVS processing software, Micheletti et al. (2014) noted a near-

doubling of RMSE when the web-based 123DCatch was used instead of Eos PhotoModeler, though this effect was removed when the point clouds were aligned using an iterative closest point algorithm (Besl and McKay, 1992). Oúedraogo et al. (2014) observed that MicMac performed better than Agisoft in a ploughed agricultural catchment as the more sophisticated camera model reduced the observed doming effect and Stumpf et al. (2015) found that MicMac outperformed VisualSfM for similar reasons. In a comparison of sensors, Thoeni et al. (2014) observed that consumer-grade digital cameras performed similarly to professional grade cameras, though GoPro devices performed less well. Micheletti et al. (2014) found that DSLR imagery and that from a camera phone produced models of a similar quality with errors of the same order of magnitude; indeed camera phone imagery even outperformed DSLR imagery in one test. Moreover, Smith and Vericat (2015) found convergent gyrocopter-based images produced a higher quality model than standard vertical UAV-based images at similar survey ranges as the doming effect was removed (James and Robson, 2014a), image blurring from vibrations was reduced and greater user-control over the images from manual camera operation enabled image overlap to be better specified.

Using aerial imagery and applying a basic refraction correction, Woodget et al. (2014) assessed the ability of SfM-MVS to obtain topography through water. Accuracy of exposed and submerged surface reconstructions was compared in four separate surveys. Average water depths were $\sim 0.15$ m, though maximum depths of $> 0.5$ m were reported. Results were promising: once refraction correction had been applied, MEs increased in only two of the four of the surveys (0.005 m to 0.053 m and 0.004 m to -0.008 m) and were lower than exposed areas in the remaining two surveys (0.044 m to 0.023 m and 0.111 m to -0.029 m) (Woodget et al., 2014).

Overall, the lack of a consistent validation methodology or a systematic campaign to validate SfM-MVS-derived models inhibits precise determination of expected errors. The flexibility of SfM-MVS as a survey tool means that many confounding variables will combine to determine the accuracy of a SfM-MVS terrain model thereby making isolation of individual error sources extremely challenging. There exists insufficient validation data to isolate and quantify the effect of each component. This is in contrast to the standardised validation strategies for MVS algorithms where the performance of each algorithm is compared for a range of freely available, high quality validation data sets (available at: http://vision.middlebury.edu/mview/; Seitz et al., 2006). However, establishing such objective reference data to benchmark approaches is more challenging for the entire SfM-MVS workflow as applied to natural environments. It is encouraging to see images and data being made available by individual studies (James and Robson, 2012); a co-ordinated attempt to host such image sets for which concurrent TLS data is available would provide a useful starting point. The recent proliferation of SfM-MVS validation studies in physical geography-facing publications is testament to the need to improve co-ordination and standardisation of such efforts.

## VI Applications of SfM-MVS in physical geography

At present, published applications of SfM-MVS in physical geography are often proof-of-concept studies. As seen in Section V, there are many papers where quantitative validation of SfM-MVS is the primary (or secondary) aim. In general, other aims can be classified into studies that either: (i) extract spatial patterns or planimetric measurements from SfM-MVS-derived orthomosaic photographs; (ii) extract three-dimensional information (volumes or topography) from SfM-MVS point clouds; or

(iii) use SfM-MVS to quantify surface change. Each aim is demonstrated in a wide variety of environmental settings and applied to address a range of problems. A brief summary is provided herein.

The ability of SfM-MVS to generate orthophotographs of the scene of interest presents a substantial advantage over TLS as they hold a wealth of information of use to physical geographers. Indeed, orthomosaic photographs created using SfM-MVS have been used to calculate the area of wildlife sampling strips (Lisein et al., 2013), to map active and relict supraglacial drainage pathways and their association with glacier structure (Rippin et al., 2015), to delineate geological faults, joints and fractures (Vasuki et al., 2014; Figure 5a) and outcrops (see Bemis et al., 2014; Figure 5f) and have been used in combination with correlations between image texture and particle grain sizes (Carbonneau et al., 2004) to derive maps of grain size distribution on an alluvial fan (de Haas et al., 2014). Certainly, there is the potential to interrogate these orthophotographs in greater detail, for example, by applying gravelometric analysis in object detection software (e.g. BASEGRAIN; Detert and Weitbrecht, 2012, 2013).

Most commonly, SfM-MVS is applied in the production of fine-resolution terrain data. A large number of studies apply SfM-MVS to coastal environments (Harwin and Lucieer, 2012; James and Quinton, 2014; Mancini et al., 2013; Ružić et al., 2014) to extract the topography of beaches, dunes or cliffs. Implementation of SfM-MVS on cliffs surfaces is particularly straightforward since their near-vertical surfaces offer advantageous viewpoints for ground-based imagery. Beyond the shore, subaqueous topography of coral reefs has been derived by Nicosevici and Garcia (2008) and Leon et al. (2015; Figure 5b). Again, advantageous viewpoints can be achieved with relative ease underwater (images were taken by a snorkeler in Leon et al., 2015); however, obtaining accurate georeferencing data underwater is more problematic, with a basic hand-held GPS device used by Leon et al. (2015). SfM-MVS has also been used to quantify properties of rock outcrops (Favalli et al., 2012) and geological hand samples (James and Robson, 2012) where a range of viewpoints can be easily acquired.

The geometry and environmental setting of fluvial surfaces presents a more challenging test of SfM. Fonstad et al. (2013) used SfM on aerial imagery to produce models of exposed topography and Dietrich (2015) used a SfM-derived orthophotograph and DEM from a helicopter-based survey to describe morphological features of a 32 km river reach. In a braided system, Javernick et al. (2014, 2015) extended this by fusing the SfM-MVS topographic model of exposed surfaces with optical bathymetric mapping also using imagery taken from a helicopter, while Woodget et al. (2014) corrected for refraction effects to extract bathymetry from SfM-MVS data directly. This method relies on the visibility of the river bed and cannot be applied where light does not penetrate to the bed. An ephemeral river setting permitted Smith et al. (2014) to extract bed topography using SfM-MVS once a flood wave had passed. This study coupled a SfM-MVS DEM with flood marks extracted from the imagery used for the SfM-MVS model and both were input into a depth-averaged 2D hydraulic model to evaluate peak flash-flood flood magnitude. Used in this way, SfM-MVS has potential to be used as part of post-flood surveys by increasing the data-acquisition rate of teams in the field and thus enabling greater spatial coverage of flood reconstructions shortly after a flood event.

Other applications of SfM-MVS are increasingly using SfM-MVS data as input into models of surface processes in this way. Javernick et al. (2015) also used SfM topographic data as input to depth-averaged 2D hydraulic model; while Westoby et al. (2015) used SfM-MVS terrain data and a 2D hydraulic model to numerically model the propagation of different glacial outburst flood scenarios as part of a hazard

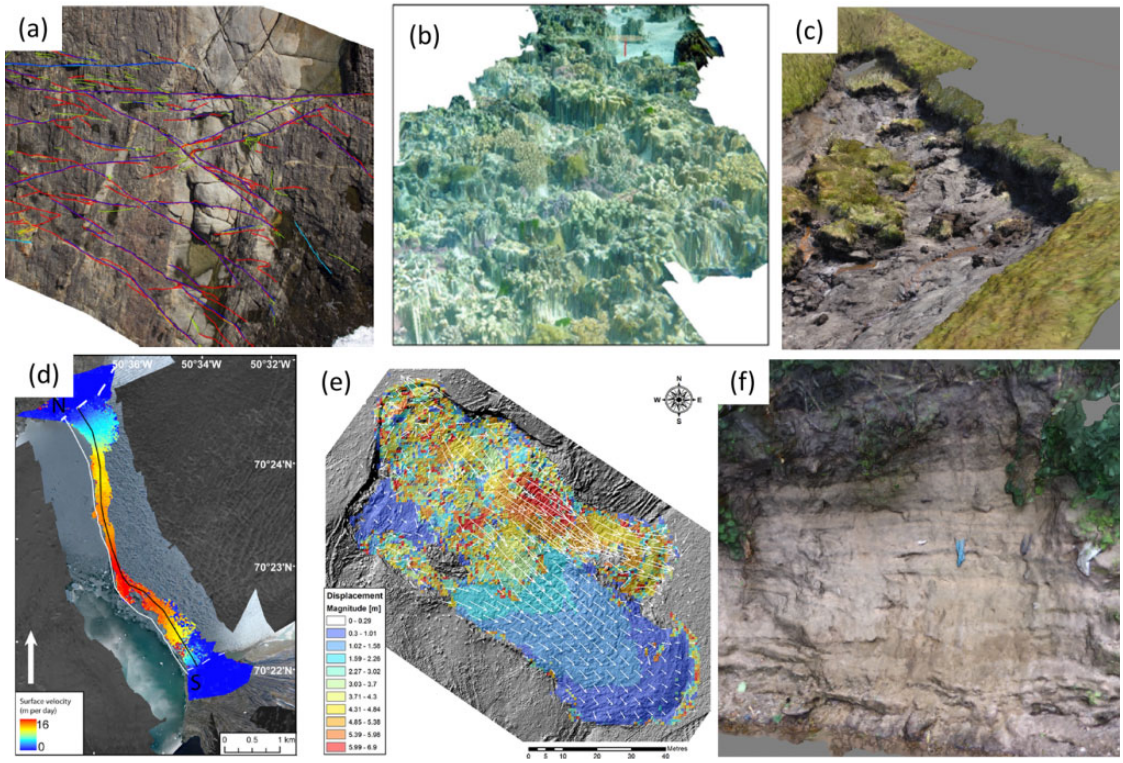


**Figure 5.** Example SfM-MVS-derived data products: (a) Faults on a rock surface detected and classified semi-automatically from an SfM-MVS orthophotograph (Vasuki et al., 2014: 29); (b) Orthophoto mosaic of an outer reef covered in live coral draped over a 1 mm resolution SfM-MVS-Digital Terrain Model (Leon et al., 2015: 4); (c) SfM-MVS 3D mesh of a peat slide; (d) Ice-flow velocities of Store Glacier, Greenland, calculated using feature tracking of SfM-MVS-DEMs (Ryan et al., 2015: 5); (d) Displacement of Holme Hill landslide calculated by applying feature tracking algorithms to SfM-MVS-derived orthomosaics (Lucieer et al., 2013: 111); (f) 3D mesh of a sedimentary sequence exposed on the River Mersey near Manchester.

assessment. Meesuk et al. (2015) fuse SfM-MVS data with ALS data, which was shown to improve the performance of urban flood models in predicting flood depth and extents. In a coastal setting Casella et al. (2014) merged SfM-MVS topography with multibeam bathymetry for input to a wave runup model. Predicted maximum wave runup was compared with that observed in SfM-MVS orthophotographs to evaluate the model. Such coupling of the topographic data created from SfM-MVS surveys with data extracted from orthophotographs has the potential expand SfM into more novel physical geography applications. For example, Lucieer et al. (2014) also combined SfM-MVS-derived topographic models and orthophotos to relate the spatial distribution and health of moss beds in East Antarctica to snowmelt drainage pathways.

Topographic data sets are often interrogated further to extract sub-grid roughness metrics (Leon et al., 2015; Rippin et al., 2015; Smith and Vericat, 2015) which are a common requirement in physical geography and related disciplines (see Smith, 2014). The large increase of data density in TLS and SfM-MVS datasets (orders of magnitude above more conventional survey techniques) permits the

calculation of roughness at a greater range of scales than before. Such roughness may influence surface processes directly (e.g. ice surface melting; Irvine-Fynn et al., 2014), reflect spatial or temporal differences in process operation (e.g. subglacial erosion and deposition; Li et al., 2010b) or be used as a surrogate for less measureable processes (e.g. flow resistance; Aberle and Smart, 2003). The increased availability of dense topographic datasets resulting from widespread application of SfM-MVS opens up the possibility of more extensive application of roughness metrics to address physical geography problems, particularly in the use of multi-scale roughness metrics (Smith, 2014).

SfM-MVS data are also used for volumetric measurement of features (Figure 5c), including the size of coastal boulders (Gienko and Terry, 2014), eroded gully volumes (Castillo et al., 2012; d'Oleire-Oltmanns et al., 2012; Frankl et al., 2015; Gómez-Gutiérrez et al., 2014) and aboveground forest biomass (Dandois and Ellis, 2013).

Repeat SfM-MVS surveys are used to monitor topographic or positional changes. Changes are quantified through: (i) interrogation of orthophotographs with image correlation software to observe displacements, as applied by Lucieer et al. (2013) to landslide displacement monitoring (Figure 5e) and Immerzeel et al. (2014) and Ryan et al. (2015) to glacier movement (Figure 5d); (ii) differencing resulting topographic models, as applied extensively in physical geography to monitor cliff retreat (James and Robson, 2012), change in periglacial sorted circles (Kääb et al., 2014), braided rivers (Tamminga et al., 2015), erosion rates of badlands (Smith and Vericat, 2015), gully volume change (Kaiser et al., 2014), rill and interrill erosion (Eltner et al., 2014), landslide activity (Stumpf et al., 2015; Turner et al., 2015), glacier thinning (Immerzeel et al., 2014), calving dynamics (Ryan et al., 2015) and lava dome subsidence (James and Varley, 2012); or (iii) by identifying 3D displacement vectors of features observed on two point clouds, as applied to study the mobility of advancing rhyolitic lava flows (Tuffen et al., 2013).

While not comprehensive, this brief overview demonstrates the range of applications for SfM-MVS in the field of physical geography and the high demand for the data provided. Physical geography is not unique in this regard. In related fields, SfM-MVS is used regularly; for example SfM-MVS is now used in archaeology (De Reu et al., 2014; McCarthy, 2014) and as part of efforts to preserve cultural heritage digitally (Gallo et al., 2014; Koutsoudis et al., 2014).

## VII Looking forward: The potential of SfM-MVS

There is little doubt that SfM-MVS surveys will play an important role in the study of physical geography into the future. It is unlikely that SfM-MVS has achieved its full potential; recent developments in computer vision and related fields indicate that SfM-MVS can address an even wider range of problems in physical geography.

Aerial platforms suitable for SfM-MVS have developed markedly in the last few years. Previous issues of image stability (Hardin and Hardin, 2010) have largely been resolved in more sophisticated UAVs on the market today. The increasing popularity of UAVs for a range of applications will likely drive down the cost of such systems. Increased battery life is improving the range and performance of UAVs. Developments in pilot-assistance and navigation systems will increase the reliability of UAVs, especially during critical take-off and landing phases. Improvement in on-board GPS systems could increase the accuracy of methods to determine camera position co-ordinates directly and avoid the need for target-based georeferencing. This development would permit SfM-MVS reconstructions of large scale

geomorphological features (e.g. alluvial fans, whole valleys) as no physical access to the study site is required. While technical issues remain relating to timing errors and the weight of onboard components required for direct georeferencing (Whitehead and Hugenholtz, 2014), these are largely being resolved. Such developments will enable SfM-MVS data acquisition over much larger areas, useful for capturing topography beyond the hillslope or feature scale and towards the landscape scale. Even routine monitoring of topographic changes over broad areas could be achieved this way. Perhaps the biggest challenge facing UAV-based SfM-MVS surveys is future legislation restricting both flight ranges and the degree of automation of such systems. With such legislation in mind, the deployment of autonomous vehicles for SfM-MVS is likely to be restricted to the ground or underwater settings. Indeed, the development of compact and cheap underwater platforms (e.g. 'OpenROV') will likely stimulate underwater applications of SfM-MVS in relatively inaccessible locations.

While the above developments enable larger areas to be incorporated into SfM-MVS surveys, static arrays of cameras can be used to monitor topographic changes over time and improve the temporal resolution of data sets. Discreet trail cameras are available for such networks and could permit truly event-scale monitoring of topographic change, useful to accurately constrain the driving forces of observed change and understand the relevant controls. Images can be transferred over the mobile network and could even be automatically input into SfM-MVS software to produce automated models of topographic change. Using such a network, image capture can be triggered by an external sensor, such as a rain or river stage gauge. Video footage could also be used in this way to ensure individual events are detected automatically thereby avoiding the need to pre-define survey intervals. Developing techniques to create models of dynamic scenes that move *during* a survey (so-called 'non-rigid' SfM; Wang et al., 2014) requires dynamic keypoint correspondences and is currently an active area of research that would have applications in studies of mass movement dynamics, for example. For field deployment, power consumption and data memory storage are both issues that need resolving. Generating topographic models 'on the fly' is computationally demanding, but could potentially be used to track the movement of objects through a scene. Video stabilisation algorithms, such as those underlying the 'hyper-lapse' videos of Kopf et al. (2014), could improve the quality of video footage taken onboard mobile platforms.

Crowd-sourcing of images for SfM has been already implemented outside of physical geography (Irschara et al., 2012; Snavely et al., 2008) and offers exciting opportunities to develop participatory science projects. In particular, hazard assessment would lend itself to such participatory methods (e.g. post-flood analysis), though issues with georeferencing, reliability, accuracy and precision remain (Boulos et al., 2011). In general, as our ability to acquire input data improves, managing data volumes and identifying efficient methods of generating and intelligently decimating point clouds (Lai et al., 2014; Morales et al., 2011) represents the main bottleneck for the future development of SfM-MVS.

## VIII Summary

By removing the necessity for either technical expertise or expensive surveying equipment, SfM has effectively democratised the acquisition of high resolution topographic data (Javernick et al., 2014). The main technical and financial limitation is the need for TS or dGPS equipment for accurate georeferencing of point clouds. The point densities and spatial resolution that are achievable with SfM-MVS are significantly greater than those of TS, dGPS, ALS and comparable to TLS; however, SfM-MVS

data are typically less precise at longer ranges (James and Robson, 2012). Reflecting this increased capacity for data capture, there has been an explosion of applications of SfM-MVS in physical geography in recent years. Survey time required in the field is minimal and the technique is sufficiently flexible to be applied over a variety of scales.

Yet, the flexibility of SfM-MVS, in terms of available platforms, sensors, data-acquisition protocols, software packages and DEM generation methods, confounds attempts to robustly validate the practically achievable data quality using SfM-MVS. A general relationship between RMSE-error and survey range has been established from a synthesis of all available quantitative validation data (Smith and Vericat, 2015), but the absence of a standardised or systematic validation strategy complicates further quantification. Indeed, the limited ability to predetermine data quality in SfM-MVS surveys and the variable success of surveys (which can only be evaluated after field campaigns are complete) is perhaps the biggest weakness in the approach.

From a detailed description of the workflow underlying SfM-MVS, it is clear that the success of SfM-MVS is determined by the specific combination of the properties of the scene and the images captured. There are a large number of complicating factors (e.g. blurring, motion, shadows, angular separation of images) that interact to determine model quality. As the workflow is often not apparent to a typical end-user, reasons for success or failure may be unclear.

Moreover, the workflow demonstrates a large number of quality thresholds that must be specified to implement SfM-MVS. For example, at the keypoint correspondence stage a 'distance ratio' criterion is used to ensure the Euclidean distance of the nearest neighbour is sufficiently distinct from the second nearest neighbour; the value specified is variable between implementations of SfM. Other thresholds relate to approximate matching of nearest neighbours for computational efficiency and the identification of geometrically inconsistent matches. At present, these are neither routinely reported nor adjusted individually by SfM-MVS-users in physical geography; rather a qualitative global quality setting is often specified in individual software packages, further encouraging a 'black box' approach to SfM-MVS. The specific implementation of SfM-MVS is often more transparent in open-source software; such transparency and ability to adjust specific parameters implemented in the workflow should be encouraged. Critical perspectives of SfM-MVS implementation in physical geography often focus on the stages that are common to conventional photogrammetry (e.g. lens model specification; James and Robson, 2014a). Greater engagement with each step of the SfM-MVS workflow will be of benefit to the physical geography community.

Nevertheless, SfM-MVS has revolutionized topographic data capture in physical geography; it has been applied in a range of environmental settings to address a number of problems. The advent of TLS in the previous decade perhaps primed the physical geography community to be especially receptive to SfM-MVS. Indeed, in common with TLS, greater interrogation and quantification of the rich data sets that arise, combined with further technological advances in sensor design, platforms and real-time topographic monitoring, indicate that the full potential of SfM-MVS in physical geography has yet to be realised.

## Acknowledgements

The authors would like to thank Damià Vericat, James Brasington and Mike James for discussions on SfM-MVS. We are grateful for the reviews provided by Mike James and two anonymous reviewers who improved the paper considerably. This paper arose from research undertaken for a forthcoming e-book entitled *Structure from Motion in the Geosciences* to

be published by Wiley-Blackwell in the *Analytical Methods in Earth and Environmental Science* series.

## Declaration of Conflicting Interests

The authors declared no potential conflicts of interest with respect to the research, authorship, and/or publication of this article.

## Funding

The authors received no financial support for the research, authorship and/or publication of this article.

## References

Aberle J and Smart GM (2003) The influence of roughness structure on flow resistance on steep slopes. *Journal of Hydraulic Research* 41: 259–269.

Ahmadabadian AH, Robson S, Boehm J, et al. (2013) A comparison of dense matching algorithms for scaled surface reconstruction using stereo camera rigs. *ISPRS Journal of Photogrammetry and Remote Sensing* 78: 157–167.

Alho P, Kukko A, Hyyppä H, et al. (2009) Application of boat-based laser scanning for river survey. *Earth Surface Processes and Landforms* 34: 1831–1838.

Arya S, Mount DM, Netanyahu NS, et al. (1998) An optimal algorithm for approximate nearest neighbour searching in fixed dimensions. *Journal of the Association for Computing Machinery* 45: 891–923.

Ballard DH and Brown CM (1982) *Computer Vision*. New Jersey: Prentice-Hall.

Bangen SG, Wheaton JM, Bouwes N, et al. (2014a) Crew variability in topographic surveys for monitoring wadeable streams: A case study from the Columbia River Basin. *Earth Surface Processes and Landforms* 39(15): 2070–2086.

Bangen SG, Wheaton JM, Bouwes N, et al. (2014b) A methodological intercomparison of topographic survey techniques for characterizing wadeable streams and rivers. *Geomorphology* 206: 343–361.

Bay H, Ess A, Tuytelaars T, et al. (2008) Speeded-up robust features (SURF). *Computer Vision and Image Understanding* 110: 346–359.

Bell ADF (2012) Section 2.3.1: Creating DEMs from surface data: Interpolation methods and determination of accuracy. In: Cook SJ, Clarke LE and Nield JM (eds) *Geomorphological Techniques* (Online Edition). London, UK: British Society for Geomorphology. ISSN: 2047-0371.

Bemis SP, Micklethwaite S, Turner D, et al. (2014) Ground-based and UAV-based photogrammetry: A multi-scale, high-resolution mapping tool for structural geology and palaeoseismology. *Journal of Structural Geology* 69: 163–178.

Bentley JL (1975) Multidimensional binary search trees used for associative searching. *Communications of the Association for Computing Machinery* 18(9): 509–517.

Besl PJ and McKay ND (1992) Method for registration of 3-D shapes. *Proceedings of the International Society for Optics and Photonics* 1611: 586–606.

Boulos MNK, Resch B, Crowley DN, et al. (2011) Crowdsourcing, citizen sensing and sensor web technologies for public and environmental health surveillance and crisis management: Trends, OGC standards and application examples. *International Journal of Health Geographics* 10(1): 67.

Brasington J, Langham J and Rumsby B (2003) Methodological sensitivity of morphometric estimates of coarse fluvial sediment transport. *Geomorphology* 53: 299–316.

Brasington J, Rumsby B and McVey R (2000) Monitoring and modelling morphological change in a braided gravel-bed river using high resolution GPS-based survey. *Earth Surface Processes and Landforms* 25(9): 973–990.

Brasington J, Vericat D and Rychkov I (2012) Modeling river bed morphology, roughness and surface sedimentology using high resolution terrestrial laser scanning. *Water Resources Research* 48: W11519, doi: 10.1029/2012WR012223.

Brodu M and Lague D (2012) 3D t-lidar data classification of complex natural scenes. *ISPRS Journal of Photogrammetric Remote Sensing* 68: 121–134.

Butler JB, Lane SN and Chandler JH (2002) Through-water close-range digital photogrammetry in flume and field experiments. *The Photogrammetric Record* 17(99): 419–439.

Calonder M, Lepetit V, Strecha C, et al. (2010) BRIEF: binary robust independent elementary features. In: Daniilidis K, Maragos P and Paragios N (eds) *Computer Vision—ECCV 2010, Lecture Notes in Computer Science* 6314. Berlin, Heidelberg: Springer, pp. 778–792.

Carbonneau PE, Lane SN and Bergeron NE (2003) Cost-effective non-metric close-range digital photogrammetry and its application to a study of coarse

gravel river beds. *International Journal of Remote Sensing* 24(14): 2837–2854.

Carbonneau PE, Lane SN and Bergeron NE (2004) Catchment-scale mapping of surface grain size in gravel bed rivers using airborne digital imagery. *Water Resources Research* 40(7): W07202.

Casella E, Rovere A, Pedroncini A, et al. (2014) Study of wave runup using numerical models and low-altitude aerial photogrammetry: A tool for coastal management. *Estuarine, Coastal and Shelf Science* 149: 160–167.

Castillo C, Pérez R, James MR, et al. (2012) Comparing the accuracy of several field methods for measuring gully erosion. *Soil Science Society of America Journal* 76(4): 1319–1332.

Cecchi E, van Wyk de Vries B, Lavest JM, et al. (2003) N-view reconstruction: A new method for morphological modelling and deformation measurement in volcanology. *Journal of Volcanology and Geothermal Research* 123: 181–201.

Chandler J (1999) Effective application of automated digital photogrammetry for geomorphological research. *Earth Surface Processes and Landforms* 24(1): 51–63.

Charlton ME, Large ARG and Fuller IC (2003) Application of airborne LiDAR in river environments: The River Coquet, Northumberland, UK. *Earth Surface Processes and Landforms* 28(3): 299–306.

Cignoni P, Rocchini C and Scopigno R (1998) Metro: Measuring error on simplified surfaces. *Computer Graphics Forum* 7(2): 167–174.

Colomina I and Molina P (2014) Unmanned aerial systems for photogrammetry and remote sensing: A review. *ISPRS Journal of Photogrammetry and Remote Sensing* 92: 79–97.

Cramer M (2004) Performance of medium format digital aerial sensor systems. *International Archives of Photogrammetry and Remote Sensing* 35: B5.

Dandois JP and Ellis EC (2010) Remote sensing of vegetation structure using computer vision. *Remote Sensing* 2: 1157–1176.

Dandois JP and Ellis EC (2013) High spatial resolution three-dimensional mapping of vegetation spectral dynamics using computer vision. *Remote Sensing of Environment* 136: 259–276.

de Haas T, Ventra D, Carbonneau PE, et al. (2014) Debris-flow dominance of alluvial fans masked by runoff reworking and weathering. *Geomorphology* 217: 165–181.

De Reu J, De Smedt P, Herremans D, et al. (2014) On introducing an image-based 3D reconstruction method in archaeological excavation practice. *Journal of Archaeological Science* 41: 251–262.

Detert M and Weitbrecht V (2012) Automatic object detection to analyze the geometry of gravel grains: A free stand-alone tool. In: Muñoz REM (ed.) *River Flow* 2012. Leiden: CRC Press / Balkema, pp. 595–600.

Detert M and Weitbrecht V (2013) User guide to gravelometric image analysis by BASEGRAIN. In: Fukuoka S, Nakagawa H, Sumi, et al. (eds) *Advances in River Sediment Research*. Leiden: CRC Press / Balkema, pp. 1789–1796.

Dietrich JT (2015) Riverscape mapping with helicopter-based Structure-from-Motion photogrammetry. *Geomorphology* doi:10.1016/j.geomorph.2015.05.008.

d'Oleire-Oltmanns S, Marzolff I, Peter KD, et al. (2012) Unmanned aerial vehicle (UAV) for monitoring soil erosion in Morocco. *Remote Sensing* 4: 3390–3416.

Dunford R, Michel K, Gagnage M, et al. (2009) Potential and constraints of unmanned aerial vehicle technology for the characterization of Mediterranean riparian forest. *International Journal of Remote Sensing* 30: 4915–4935.

Eltner A, Baumgart P, Maas HG, et al. (2014) Multitemporal UAV data for automatic measurement of rill and interrill erosion on loess soil. *Earth Surface Processes and Landforms* 40(6): 741–755. doi: 10.1002/esp.3673.

Evans M and Lindsay J (2010) High resolution quantification of gully erosion in upland peatlands at the landscape scale. *Earth Surface Processes and Landforms* 35: 876–886.

Favalli M, Fornaciai A, Isola I, et al. (2012) Multiview 3D reconstruction in geosciences. *Computers & Geosciences* 44: 168–176.

Fischler MA and Bolles RC (1981) Random sample consensus: A paradigm for model fitting with applications to image analysis and automated cartography. *Communications of the Association for Computing Machinery* 24(6): 381–395.

Fonstad MA, Dietrich JT, Courville BC, et al. (2013) Topographic structure from motion: A new development in photogrammetric measurement. *Earth Surface Processes and Landforms* 38: 421−430.

Frankl A, Stal C, Abraha A, et al. (2015) Detailed recording of gully morphology in 3D through image-based modelling. *Catena* 127: 92–101.

Friedman JH, Bentley JL and Finkel RA (1977) An algorithm for finding best matches in logarithmic expected time. *ACM Transactions on Mathematical Software* 3: 209–226.

Fuller IC, Large ARG, Charlton ME, et al. (2003) Reach-scale sediment transfers: An evaluation of two morphological budgeting approaches. *Earth Surface Processes and Landforms* 28: 889–903.

Furukawa Y and Ponce J (2009) Carved visual hulls for image-based modelling. *International Journal of Computer Vision* 81: 53−67.

Furukawa Y and Ponce J (2010) Accurate, dense and robust multiview stereopsis. *IEEE Transactions on Pattern Analysis and Machine Intelligence* 32: 1362−1376.

Furukawa Y, Curless B, Seitz SM, et al. (2010) Towards internet-scale multi-view stereo. In: *Computer Vision and Pattern Recognition (CVPR)*, 13–18 June, San Francisco, CA, USA, pp. 1434–1441. IEEE Conference.

Gallay M (2013) Section 2.1.4: Direct acquisition of data: Airborne laser scanning. In: Cook SJ, Clarke LE and Nield JM (eds) *Geomorphological Techniques* (Online Edition). London, UK: British Society for Geomorphology. ISSN: 2047-0371.

Gallo A, Muzzupappa M and Bruno F (2014) 3D reconstruction of small sized objects from a sequence of multi-focused images. *Journal of Cultural Heritage* 15(2): 173–182.

Gienko GA and Terry JP (2014) Three-dimensional modeling of coastal boulders using multi-view image measurements. *Earth Surface Processes and Landforms* 39(7): 853–864.

Gómez-Gutiérrez Á, Schnabel S, Berenguer-Sempere F, Lavado-Contador F, Rubio-Delgado J, et al. (2014) Using 3D photo-reconstruction methods to estimate gully headcut erosion. *Catena* 120: 91–101.

Granshaw SI (1980) Bundle adjustment methods in engineering photogrammetry. *The Photogrammetric Record* 10: 181–207.

Hardin PJ and Hardin TJ (2010) Small-scale remotely piloted vehicles in environmental research. *Geography Compass* 4(9): 1297–1311.

Hartley R and Zisserman A (2003) *Multiple View Geometry in Computer Vision*. Cambridge: Cambridge University Press.

Hartley RI and Sturm P (1997) Triangulation. *Computer Vision and Understanding* 68: 146–157.

Harwin S and Lucieer A (2012) Assessing the accuracy of georeferenced point clouds produced via multi-view stereopsis from unmanned aerial vehicle (UAV) imagery. *Remote Sensing* 4(6): 1573–1599.

Hetherington D, Heritage G and Milan D (2005) Reach scale sub-bar dynamics elucidated through oblique lidar survey. *International Association of Hydrological Science*. Red Book Publication 291. 278–284.

Hodge R, Brasington J and Richards K (2009) In situ characterisation of grain-scale fluvial morphology using terrestrial laser scanning. *Earth Surface Processes and Landforms* 34: 954–968.

Immerzeel WW, Kraaijenbrink PDA, Shea JM, et al. (2014) High-resolution monitoring of Himalayan glacier dynamics using unmanned aerial vehicles. *Remote Sensing of Environment* 150: 93–103

Irschara A, Zach C, Klopschitz M, et al. (2012) Large-scale, dense city reconstruction from user-contributed photos. *Computer Vision and Image Understanding* 116(1): 2–15.

Irvine-Fynn TDL, Sanz-Ablanedo E, Rutter N, et al. (2014) Measuring glacier surface roughness using plot-scale, close-range digital photogrammetry. *Journal of Glaciology* 60: 957–969.

James MR and Quinton JN (2014) Ultra-rapid topographic surveying for complex environments: The hand-held mobile laser scanner (HMLS). *Earth Surface Processes and Landforms* 39: 138–142.

James MR and Robson S (2012) Straightforward reconstruction of 3D surfaces and topography with a camera: Accuracy and geoscience application. *Journal of Geophysical Research: Earth Surface* 117: F03017. doi: 10.1029/2011JF002289.

James MR and Robson S (2014a) Mitigating systematic error in topographic models derived from UAV and ground-based image networks. *Earth Surface Processes and Landforms* 39(10): 1413–1420. doi: 10.1002/esp.3609.

James MR and Robson S (2014b) Sequential digital elevation models of active lava flows from ground-based stereo time-lapse imagery. *ISPRS Journal of Photogrammetry and Remote Sensing* 97: 160–170.

James MR and Varley N (2012) Identification of structural controls in an active lava dome with high resolution DEMs: Volcán de Colima, Mexico. *Geophysical Research Letters* 39: L22303. doi: 10.1029/2012GL054245.

James MR, Robson S, Pinkerton H, et al. (2006) Oblique photogrammetry with visible and thermal images of active lava flows. *Bulletin of Volcanology* 69: 105−108.

Javernick L, Brasington J and Caruso B (2014) Modelling the topography of shallow braided rivers using Structure-from-Motion photogrammetry. *Geomorphology* 213: 166–182. doi:10.1016/j.geomorph.2014.01.006.

Javernick L, Hicks DM, Measures R, et al. (2015) Numerical modelling of braided rivers with Structure-from-Motion-derived terrain models. *River Research and Applications* doi: 10.1002/rra.2918.

Kääb A, Girod LMR and Berthling IT (2014) Surface kinematics of periglacial sorted circles using structure-from-motion technology. *The Cryosphere* 8: 1041–1056.

Kaiser A, Neugirg F, Rock G, et al. (2014) Small-scale surface reconstruction and volume calculation of soil erosion in complex Moroccan gully morphology using Structure from Motion. *Remote Sensing* 6(8): 7050–7080.

Kopf J, Cohen MF and Szeliski R (2014) First-person hyper-lapse videos. *ACM Transactions on Graphics* 33: 78.

Koutsoudis A, Vidmar B, Ioannakis G, et al. (2014) Multi-image 3D reconstruction data evaluation. *Journal of Cultural Heritage* 15: 73−79.

Lague D, Brodu N and Leroux J (2013) Accurate 3D comparison of complex topography with terrestrial laser scanner: Application to the Rangitikei canyon (N-Z). *ISPRS Journal of Photogrammetric Remote Sensing* 82: 10–26.

Lai P, Samson C and Bose P (2014) Visual enhancement of 3D images of rock faces for fracture mapping. *International Journal of Rock Mechanics and Mining Sciences* 72: 325–335.

Lane SN (2000) The measurement of river channel morphology using digital photogrammetry. *The Photogrammetric Record* 16: 937–961.

Lejot J, Delacourt C, Piégay H, et al. (2007) Very high spatial resolution imagery for channel bathymetry and topography from an unmanned mapping controlled platform. *Earth Surface Processes and Landforms* 32(11): 1705–1725.

Leon JX, Roelfsema CM, Saunders MI, et al. (2015) Measuring coral reef terrain roughness using 'Structure-from-Motion' close-range photogrammetry. *Geomorphology* doi:10.1016/j.geomorph.2015.01.030.

Lhuillier M and Quan L (2005) A quasi-dense approach to surface reconstruction from uncalibrated images. *IEEE Transactions on Pattern Analysis and Machine Intelligence* 27: 418−433.

Li J, Li E, Chen Y, et al. (2010a) Bundled depth-map merging for multi-view stereo. In: *Computer Vision and Pattern Recognition (CVPR)*, 13–18 June 2010, San Francisco, CA, USA, pp. 2769–2776. IEEE Conference.

Li X, Sun B, Siegert MJ, et al. (2010b) Characterization of subglacial landscapes by a two-parameter roughness index. *Journal of Glaciology* 56: 831–836.

Lisein J, Linchant J, Lejeune P, et al. (2013) Aerial surveys using an unmanned aerial system (UAS): Comparison of different methods for estimating the surface area of sampling strips. *Tropical Conservation Science* 6(4).

Longuet-Higgins HC (1981) A computer algorithm for reconstructing a scene from two projections. *Nature* 293: 133–135.

Lowe DG (1999) Object recognition from local scale-invariant features. In: *International Conference on Computer Vision*, 20–27 September 1999, Kerkyra, pp. 1150–1157. Corfu, Greece.

Lowe DG (2001) Local feature view clustering for 3D object recognition. In: *Proceedings of the IEEE Conference on Computer Vision and Pattern Recognition*, 8–14 December 2001. Kauai, Hawaii.

Lowe DG (2004) Distinctive image features from scale-invariant keypoints. *International Journal of Computer Vision* 60: 91–110.

Lucieer A, de Jong SM and Turner D (2013) Mapping landslide displacements using Structure from Motion (SfM) and image correlation of multi-temporal UAV photography. *Progress in Physical Geography* 38: 97–116.

Lucieer A, Turner D, King DH, et al. (2014) Using an unmanned aerial vehicle (UAV) to capture micro-topography of Antarctic moss beds. *International Journal of Applied Earth Observation and Geoinformation* 27: 53–62.

McCarthy J (2014) Multi-image photogrammetry as a practical tool for cultural heritage survey and community engagement. *Journal of Archaeological Science* 43: 175−185.

Mancini F, Dubbini M, Gattelli M, et al. (2013) Using unmanned aerial vehicles (UAV) for high-resolution reconstruction of topography: The structure from motion approach on coastal environments. *Remote Sensing* 5(12): 6880–6898.

Meesuk V, Vojinovic Z, Mynett AE, et al. (2015) Urban flood modelling combining top-view LiDAR data with ground-view SfM observations. *Advances in Water Resources* 75: 105–117.

Micheletti N, Chandler JH and Lane SN (2014) Investigating the geomorphological potential of freely available

and accessible Structure-from-Motion photogrammetry using a smartphone. *Earth Surface Processes and Landforms* 40(4): 473–486. doi: 10.1002/esp.3648.

Micheletti N, Chandler JH and Lane SN (2015) Section 2.2. Structure from Motion (SfM) photogrammetry. In: Cook SJ, Clarke LE and Nield JM (eds) *Geomorphological Techniques* (Online Edition). London, UK: British Society for Geomorphology. ISSN: 2047-0371.

Micusik B and Pajdla T (2006) Structure from motion with wide circular field of view cameras. *IEEE Transactions on Pattern Analysis and Machine Intelligence* 28(7): 1135–1149.

Mikolajczyk K, Tuytelaars T, Schmid C, et al. (2005) A comparison of affine region detectors. *International Journal of Computer Vision* 65(1/2): 43–72.

Milne JA and Sear D (1997) Modelling river channel topography using GIS. *International Journal of Geographical Information Science* 11: 499–519.

Morales R, Wang Y and Zhang Z (2011) Unstructured point cloud surface denoising and decimation using distance RBF K-nearest neighbor Kernel. In: Morales R, Wang Y and Zhang Z (eds) *Advances in Multimedia Information Processing-PCM 2010*. Berlin Heidelberg: Springer, pp. 214–225.

Moreels P and Perona P (2007) Evaluation of features detectors and descriptors based on 3D objects. *International Journal of Computer Vision* 73(3): 263–284.

Morel J and Yu G (2009) ASIFT: A new framework for fully affine invariant image comparison. *Society for Industrial and Applied Mathematics Journal on Imaging Sciences* 2: 438–469.

Muja M and Lowe DG (2009) Fast approximate nearest neighbours with automatic algorithm configuration. In: *Proceedings of the International Conference on Computer Vision Theory and Applications (VISAPP'09)*, 5–8 February, pp. 331–340. Lisboa, Portugal.

Nicosevici T and Garcia R (2008) Online robust 3D mapping using structure from motion cues. In *MTS/IEEE Oceans*, 1–7, April 2008, Quebec, Canada.

Nistér D (2004) An efficient solution to the five-point relative pose problem. *IEEE Transactions on Pattern Analysis and Machine Intelligence* 26: 756–777.

Oúedraogo MM, Degré A, Debouche C, et al. (2014) The evaluation of unmanned aerial systems-based photogrammetry and terrestrial laser scanning to generate DEMs of agricultural watersheds. *Geomorphology* 214: 339–355. doi: 10.1016/j.geomorph.2014.02.016.

Pons J-P, Keriven R and Faugeras O (2007) Multi-view stereo reconstruction and scene flow estimation with a global image-based matching score. *International Journal of Computer Vision* 72: 179−193.

Rippin DM, Pomfret A and King N (2015) High resolution mapping of supraglacial drainage pathways reveals link between micro-channel drainage density, surface roughness and surface reflectance. *Earth Surface Processes and Landforms* 40: 1279–1290. doi: 10.1002/esp.3719.

Rosnell T and Honkavaara E (2012) Point cloud generation from aerial image data acquired by a quadrocopter type micro unmanned aerial vehicle and a digital still camera. *Sensors* 12(1): 453–480.

Ružić I, Marović I, Benac Č, et al. (2014) Coastal cliff geometry derived from structure-from-motion photogrammetry at Stara Baška, Krk Island, Croatia. *Geo-Marine Letters* 34(6): 555–565.

Ryan JC, Hubbard AL, Box JE, et al. (2015) UAV photogrammetry and structure from motion to assess calving dynamics at Store Glacier, a large outlet draining the Greenland ice sheet. *The Cryosphere* 9(1): 1–11.

Rychkov I, Brasington J and Vericat D (2012) Computational and methodological aspects of terrestrial surface analysis based on point clouds. *Computers & Geosciences* 42: 64–70.

Seitz S and Dyer C (1999) Photorealistic scene reconstruction by voxel coloring. *International Journal of Computer Vision* 35(2): 151–173.

Seitz SM, Curless B, Diebel J, et al. (2006) A comparison and evaluation of multi-view stereo reconstruction algorithms in computer vision and pattern recognition. *IEEE Computer Society Conference* 1: 519–528.

Smith MW (2014) Roughness in the earth sciences. *Earth Science Reviews* 136: 202–225.

Smith MW (2015) Section 2.1.5: Direct acquisition of elevation data: Terrestrial Laser Scanning. In: Cook SJ, Clarke LE and Nield JM (eds) *Geomorphological Techniques* (Online Edition). London, UK: British Society for Geomorphology. ISSN: 2047-0371.

Smith MW and Vericat D (2015) From experimental plots to experimental landscapes: Topography, erosion and deposition in sub-humid badlands from Structure-from-Motion photogrammetry. *Earth Surface Processes & Landforms* 40: 1656–1671. doi:10.1002/esp.3747.

Smith MW, Carrivick JL, Hooke J, et al. (2014) Reconstructing flash flood magnitudes using 'Structure-from-

Motion': A rapid assessment tool. *Journal of Hydrology* 519: 1914–1927.

Snavely N (2008) Scene Reconstruction and Visualization from Internet Photo Collections. PhD thesis, University of Washington, USA.

Snavely N, Seitz SN and Szeliski R (2008) Modeling the world from Internet photo collections. *International Journal of Computer Vision* 80: 189–210.

Strecha C, Bronstein A, Bronstein M, et al. (2012) LDA-Hash: Improved matching with smaller descriptors. *IEEE Transactions on Pattern Analysis and Machine Intelligence* 34: 66–78.

Stumpf A, Malet JP, Allemand P, et al. (2015) Ground-based multi-view photogrammetry for the monitoring of landslide deformation and erosion. *Geomorphology* 231: 130–145.

Szeliski R (2011) *Computer Vision: Algorithms and applications*. London: Springer.

Tamminga AD, Eaton BC and Hugenholtz CH (2015) UAS-based remote sensing of fluvial change following an extreme flood event. *Earth Surface Processes and Landforms* 40: 1464–1476. doi: 10.1002/esp.3728.

Tarolli P (2014) High-resolution topography for understanding Earth surface processes: Opportunities and challenges. *Geomorphology* 216: 295–312.

Thoeni K, Giacomini A, Murtagh R, et al. (2014) A comparison of multi-view 3D reconstruction of a rock wall using several cameras and a laser scanner. In: *Proceedings of ISPRS Technical Commission V Symposium*, 23–25 June 2014, Riva del Garda, Italy.

Thommeret N, Bailly JS and Puech C (2010) Robust extraction of thalwegs network from DTM: Application on badlands. *Hydrology and Earth System Sciences Discussion* 7: 879–905.

Tonkin TN, Midgley NG, Graham DJ, et al. (2014) The potential of small unmanned aircraft systems and structure-from-motion for topographic surveys: A test of emerging integrated approaches at Cwm Idwal, North Wales. *Geomorphology* 226: 35–43. doi: 10.1016/j.geomorph.2014.07.021.

Torr PHS and Zisserman A (2000) MLESAC: A new robust estimator with application to estimating image geometry. *Computer Vision and Image Understanding* 78: 138–156.

Triggs B, McLauchlan PF, Hartley RI, et al. (2000) Bundle adjustment: A modern synthesis. In: Triggs B, Zisserman A and Szeliski R (eds) *Vision Algorithms '99*, LNCS 1883. Berlin Heidelberg: Springer-Verlag, pp. 298–372.

Tsai ML, Chiang KW, Huang YW, et al. (2010) The development of a direct georeferencing ready UAV based photogrammetry platform. In: *Proceedings of the 2010 Canadian Geomatics Conference and Symposium of Commission I*, Calgary, AB, Canada, 15–18 June 2010.

Tuffen H, James MR, Castro JM, et al. (2013) Exceptional mobility of an advancing rhyolitic obsidian flow at Cordon Caulle volcano in Chile. *Nature Communications* 4: 2709. doi: 10.1038/ncomms3709.

Turner D, Lucieer A and de Jong SM (2015) Time series analysis of landslide dynamics using an unmanned aerial vehicle (UAV). *Remote Sensing* 7(2): 1736–1757.

Turner D, Lucieer A and Wallace L (2014) Direct georeferencing of ultrahigh-resolution UAV imagery. *IEEE Transactions on Geoscience and Remote Sensing* 52: 2738–2745.

Ullman S (1979) The interpretation of Structure from Motion. *Proceedings of the Royal Society B* 203: 405–426.

Unger J, Reich M and Heipke C (2014) UAV-based photogrammetry: Monitoring of a building zone. *The International Archives of the Photogrammetry, Remote Sensing and Spatial Information Sciences*, Volume XL-5, 2014 ISPRS Technical Commission V Symposium, 23–25 June 2014, Riva del Garda, Italy.

Vasuki Y, Holden EJ, Kovesi P, et al. (2014) Semi-automatic mapping of geological structures using UAV-based photogrammetric data: An image analysis approach. *Computers & Geosciences* 69: 22–32.

Verhoeven GJ, Loenders J, Vermeulen F, et al. (2009) Helikite aerial photography: A versatile means of unmanned, radio controlled, low-altitude aerial archaeology. *Archaeological Prospection* 16(2): 125–138.

Vericat D, Brasington J, Wheaton J, et al. (2009) Accuracy assessment of aerial photographs acquired using lighter-than-air blimps: Low-cost tools for mapping river corridors. *River Research and Applications* 25(8): 985–1000.

Wang YM, Zheng JB, Jiang MF, et al. (2014) A trajectory basis selection method for nonrRigid Structure from Motion. *Applied Mechanics and Materials* 644–650: 1396–1399.

Westaway RM, Lane SN and Hicks DM (2000) The development of an automated correction procedure for

digital photogrammetry for the study of wide, shallow, gravel-bed rivers. *Earth Surface Processes and Landforms* 25: 209–226.

Westoby MJ, Brasington J, Glasser NF, et al. (2012) 'Structure-from-Motion' photogrammetry: A low-cost, effective tool for geoscience applications. *Geomorphology* 179: 300−314.

Westoby MJ, Brasington J, Glasser NF, et al. (2015) Numerical modelling of glacial lake outburst floods using physically based dam-breach models. *Earth Surface Dynamics* 3(1): 171–199.

Wheaton JM, Brasington J, Darby SE, et al. (2010) Accounting for uncertainty in DEMs from repeat topographic surveys: Improved sediment budgets. *Earth Surface Processes and Landforms* 35(2): 136–156.

Whitehead K and Hugenholtz CH (2014) Remote sensing of the environment with small unmanned aircraft systems (UASs). Part 1: A review of progress and challenges. *Journal of Unmanned Vehicle Systems* 2(3): 69–85.

Woodget AS, Carbonneau PE, Visser F, et al. (2014) Quantifying submerged fluvial topography using hyperspatial resolution UAS imagery and structure from motion photogrammetry. *Earth Surface Processes and Landforms* 40: 47–64. doi: 10.1002/esp.3613.

Young EJ (2012) Section 2.1.3 dGPS. In: Cook SJ, Clarke LE and Nield JM (eds) *Geomorphological Techniques* (Online Edition). London, UK: British Society for Geomorphology. ISSN: 2047-0371.

Zahawi RA, Dandois JP, Holl KD, et al. (2015) Using lightweight unmanned aerial vehicles to monitor tropical forest recovery. *Biological Conservation* 186: 287–295.